2016

Exploration of grating-based surface plasmon resonance systems for wave vector matching to enhance plasmon modes and preliminary surface plasmon-enhanced fluorescence interrogation

Michael B. Johnson
Iowa State University

Exploration of grating-based surface plasmon resonance systems for wave vector matching to enhance plasmon modes and preliminary surface plasmon-enhanced fluorescence interrogation

by

Michael B. Johnson

A thesis submitted to the graduate faculty

in partial fulfillment of the requirements for the degree of

MASTER OF SCIENCE

Major: Chemical Engineering

Program of Study Committee:
Andrew Hillier, Major Professor
Emily Smith
Matthew Panthani

Iowa State University

Ames, Iowa

2016

TABLE OF CONTENTS

Page

NOMENCLATURE iv
ACKNOWLEDGMENTS v

ABSTRACT..... vi

CHAPTER 1 INTRODUCTION TO SURFACE PLASMON RESONANCE.... 1

1.1 Surface Plasmon Resonance Interests and Application Fields 1
1.2 Wave Vector Coupling from Light to Surface Bound Modes in SPR..... 5
1.3 Wave Vector Matching through Refractive Index Matching 14
1.4 Fluorescence Enhancement..... 17
1.5 References..... 20

CHAPTER 2 HIGH REFRACTIVE INDEX SURFACE PLASMON WAVE VECTOR MATCHING ACROSS A THIN METAL FILM GRATING PROBED WITH REFRACTIVE INDEX SENSING 25

2.1 Abstract 25
2.2 Introduction..... 26
2.3 Experimental Section..... 29
2.3.1 Materials 29
2.3.2 Grating Fabrication 29
2.3.3 Ellipsometry..... 30
2.3.4 Optical Characterization 30
2.3.5 Refractive Index Sensing..... 31
2.3.5 Optical Modeling 31
2.4 Results and Discussion 32
2.4.1 Orientation to Results: Fabrication and Optical Experiments 32
2.4.2 Normal (θ=0°), Unmatched Transmission Spectra Introduction 33
2.4.3 Increasing High RI Thickness Transmission Spectra 35
2.4.4 Increasing High RI Thickness Computational Analysis..... 37
2.4.5 Probing Matched and Unmatched System with RI Sensing 39
2.5 Conclusion 40
2.6 Acknowledgements..... 41
2.7 Supporting Information..... 41
2.7.1 Additional Results: Dispersion Images and Simulations..... 41
2.7.2 Thin Film Analysis: Ellipsometry..... 45
2.7.3 RCWA Modeling..... 48
2.8 References..... 49

CHAPTER 3 FLUORESCENCE ENHANCEMENT OF ABSORPTION AND EMISSION MODES OF RHODAMINE B IN POLY(METHYL METHACRYLATE) THROUGH SURFACE PLASMON COUPLED VIA SILVER GRATINGS 54

3.1 Abstract 54
3.2 Introduction 54
3.3 Experimental Section 56
3.3.1 Materials 56
3.3.2 Grating Fabrication 57
3.3.3 PMMA/RhB Spin Preparation and Coating 57
3.3.4 Optical Characterization 58
3.4 Results and Discussion 59
3.4.1 Orientation to Results: Samples Analyzed and Spectral Results 59
3.4.2 RhB in Ethanol Spectra and Band Pass Filter Analysis 59
3.4.3 Dispersion Images 61
3.4.4 Fluorescence Spectra 63
3.5 Conclusion 64
3.6 Proposed Study 65
3.7 Acknowledgements 66
3.8 References 66

NOMENCLATURE

SPR	Surface Plasmon Resonance
LSPR	Localized Surface Plasmon Resonance
LRSPR	Long Range Surface Plasmon Resonance
SRPSPR	Short Range Surface Plasmon Resonance
TIR	Total Internal Reflection
RI	Refractive Index
SERS	Surface Enhanced Raman Spectroscopy
SEIRA	Surface Enhanced Infrared Absorption
MEF	Metal Enhanced Fluorescence
SPEA	Surface Plasmon Enhanced Absorption
SPCE	Surface Plasmon Coupled Emission

ACKNOWLEDGMENTS

I would like to begin by dedicating this thesis to my friends and family who have given me the fortitude to make it this far. Thank you to my PI and research professor, Dr. Andrew Hillier, and his NSF supporters for funding this project. Thank you to my teachers and current and former committee members, Dr. Emily Smith, Dr. Meng Lu, Dr. Surya Mallapragada, Dr. Liang Dong, and Dr. Matthew Panthani. Thank you to the previous graduate students in my lab, Dr. Joseph Petefish and Dr. Subramanian Venkatachalam, who first hand helped me get into my research project, as well as previous graduate influences in our lab before my time, Dr. Bipin Singh and Dr. Wei-Hsun Yeh. Thank you to Iowa State University, the Graduate College, the College of Engineering, the Chemical and Biological Engineering (CBE) department (including faculty, department staff and our DoGEs), as well as other departments (Chemistry, Electrical Engineering, Physics and Ames Lab) for the education and guidance I have received while pursuing this Master's Degree. Finally, thank you to the CBE graduate student body, and other graduate student supporters, who helped me achieve this.

ABSTRACT

Surface plasmon resonance refers to the collective oscillation of conductance band electrons in a metal. The most common experimental method to excite surface plasmon resonance is with light through a coupling mode (prism, grating, waveguide, etc). The work presented in this thesis uses experimental observations of surface plasmon resonance, bolstered with theoretical, analytical and computational solutions, in order to explain and show applications of the phenomena observed.

Chapter 1 introduces surface plasmon resonance by explicating historical interest in the phenomena. Theoretical and experimental results opened the door for surface plasmon resonance to be used as a refractive index sensor (allowing for diagnostics and kinetics studies). Surface plasmon resonance is also associated with a highly localized electric field, which can be used to enhance many spectroscopic techniques like infrared absorption, fluorescence, Raman spectroscopy, and surface chemistry reactions. This chapter will close by looking into the specific information on studies that will be found in subsequent chapters.

Chapter 2 reveals information behind a study conducted to increase the localization of light in a surface plasmon resonance system through matching the surface plasmon resonance wave vectors across a thin metal film. As discussed in depth, this matching occurs by shifting the front side optical properties to match the back side (across the metal film), through the use of a high refractive index layer. Finally, this system is probed with refractive index sensing of the new (matched- high refractive index film present) sensor, and native (unmatched- no high refractive index film) sensor.

Chapter 3 introduces a study laying ground work in future experiments in our lab pertaining to enhancing photoluminescence with surface plasmon resonance. Preliminary data shows enhanced fluorescence of rhodamine B in poly(methyl methacrylate) thin films due to the films' proximity to metal gratings. Implications of the preliminary findings are explicated and a full study is proposed.

CHAPTER 1

INTRODUCTION TO SURFACE PLASMON RESONANCE

1.1 Surface Plasmon Resonance Interests and Application Fields

The first recorded observation of surface plasmon resonance (SPR) was discovered over 100 years ago, when Wood noticed polarized light shone on metallic gratings produced extraordinary light and dark bands.[1,2] Lord Rayleigh introduced the first theoretical treatment of these anomalies through his work in 1907,[3] and subsequent theoretical and experimental work emerged slowly throughout the century.[4] By the 1960s, experiments had been performed analyzing the energy loss of electrons in thin metal foils.[5,6] Pines and Bohm suggested that the energy losses in metal foils are due to excitation of conduction band electrons, creating plasma oscillations or plasmons.[7–9] It was later discovered that plasmon generation and associated energy loss is due to the extension of the electric field beyond the boundary of the specimen.[6] This meant that any presence of a film, or contaminant on the plasmonic specimen surface would alter the plasmon. This phenomena was classified as an evanescent wave at the surface of the metal.[10]

Original applicability of SPR was demonstrated in the late 1960s with prism-based coupling for refractive index (RI) sensing.[11–13] Early applications in this area were pioneered by Nylander and Liedberg.[14] Prism based SPR results in a single resonance (absorption) peak at an angle larger than that for total internal reflection (TIR). This peak can be tracked in either angle or wavelength interrogation, allowing for its use for characterizing thin films[15,16] and biological and chemical sensing.[17,18] While the resonance peak may be sharp, the angle where the peak occurs is usually large and is restricted by the RI of the prism. Returning to

the original motivation and discovery of SPR, periodic gratings have gained prominence as an SPR sensing platform since the 1970s.[19–21] These periodic gratings offer more tunability in terms of angle of impingement and regime of SPR excitation. They also provide multiple orders of diffracted light coupling to SPR, as well as out coupling of light, in which SPR is allowed to couple to radiative mode for additional information extraction.

A distinction should be made here between localized SPR (LSPR) and propagating SPR. This far, propagating SPR modes have been discussed. However, LSPR exists on nanoparticles (NPs) such as nanometer scale spheres and rods dispersed in solution.[22–24] The electron clouds of these particles oscillate around the mass center of the particle with traversing EM waves. LSPR will not be the focus of this report. Further discussions will assume propagating SPR when referring to SPs and SPR in general.

The advantages and disadvantages for SPR and its different excitation modes are numerous and typically depend on the sensing application.[25] SPR offers such robust sensing capabilities due to a sensitivity to the local optical properties that exist within the evanescent wave. This RI sensitivity allows for high throughput label free sensing/diagnostics[26–31] and thin film deposition tracking.[32–40] Additionally, because SPR peak shift can be tracked versus time, kinetics and binding affinity can be elucidated.[19,41,42] The first commercial SPR instrument for binding affinity was sold in 1990 under the name of BIACORE.[43–45] BIACORE is still sold today as a subsidiary of General Electrics.

Additionally, the enhanced electric field associated with the resonance mode can be matched to atomic or molecular resonance Spectroscopic techniques enhanced by SPR include Surface Enhanced Raman Spectroscopy (SERS),[34,46–50] Surface Enhanced Infrared Absorption (SEIRA),[36,47,51,52] and SPR enhanced fluorescent signaling.[53–61] SPR also plays an

integral role in near-field imaging techniques.[62,63] Experiments show SPR can also monitor and/or drive surface catalyzed reactions.[34,46] SPR can also facilitate solar energy conversion.[64–68] A table highlighting the types of application fields for SPR is shown in Figure 1.1.

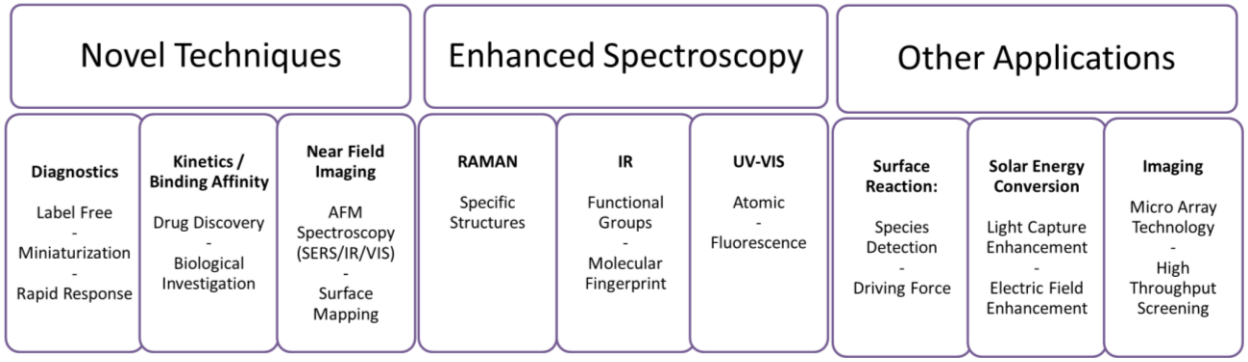

Figure 1.1 Application fields for surface plasmon resonance.

A major limitation of SPR is due to the loss of light, or absorption of light, in metals. Not only is some light lost due to absorption, it also increases resonance peak width.[69] Additionally, roughness effects,[70–72] oxidation/corrosion,[6,73] and cost of noble metals create difficulty in implementing long lasting, low cost, reproducible SPR sensors. Another limitation of SPR is that spatial resolution can be poor due to the propagation length of the surface plasmon along the metal dielectric interface.[42,74]

This report focuses mainly on grating based excitation, due to the advantageous tunability and multiple diffractive orders that can excite SPs.[75] Gratings also reemit light, from SP modes coupling to propagating light, allowing for extraction of information on how light interacts with the sensor.[76,77] Also, nanostructures offer a wide breadth of applications

through the diversity of structures which can excite surface plasmons (arrays of holes,[78,79] pyramids,[80] pillars,[81,82] and various grating structures[72]).

Consider the case of a one dimensional (1D) gratings (periodicity in one direction). The plasmonic response will vary greatly between perfectly sinusoidal, broad bumps, spikes or box gratings.[72] Additionally, variations in the amplitude (height of structures) and pitch (distance between periodic structures) greatly affect the enhancement.[75] Additionally, structures must be optimized to the wavelength of light to be used and the angle of incidence desired.

Additional to type of periodic structure and specific geometry, the substrate composition and optical properties effects the surface plasmon quality, as does the type of nobel metal used (Ag, Au and Al).[69,83] Additional to the optical properties of materials being a concern, physical limitations of certain materials exist, such as the corrosion of Ag,[73,74,84] the difficulty of adhesion of Au,[26,79,85,86] and the oxide formation of Al.[6]

Finally, while state of the art fabrication techniques allow researchers to modulate surfaces to probe plasmonic responses by fine tuning parameters, it is nearly impossible to probe the field of nanostructures possible (variations in shape/geometry, symmetry, amplitude, periodicity, etc). This has motivated the formulation of fast converging computational models to offer researchers with a deeper understanding of plasmonic responses.[87–89] With computational models, orders of magnitude more experiments can be performed in the same time it would take to perform one experiment in lab, without the convolution due to physical experimental issues like surface roughness, oxidation, and corrosion.

1.2 Wave Vector Coupling from Light to Surface Bound Modes in SPR

Surface plasmons (SPs) refer to oscillations of free electron density near a metal-dielectric interface. This collective oscillation and propagation of surface bound modes is called surface plasmon resonance (SPR).[5,11,13] SPR is excited by electromagnetic (EM) waves coupled to the surface bound mode through various coupling methods. When coupled, the resultant surface bound mode has electric field oscillations perpendicular to the metal-dielectric interface (E_z), magnetic field oscillations in the plane of the metal-dielectric interface (H_y) and a propagation in the positive x-direction (E_x), as shown in Figure 1.2. This means that when using light to excite SPR, it must be p-polarized or transverse magnetic (TM), with the magnetic field oscillating in the plane of the interface.[25,90]

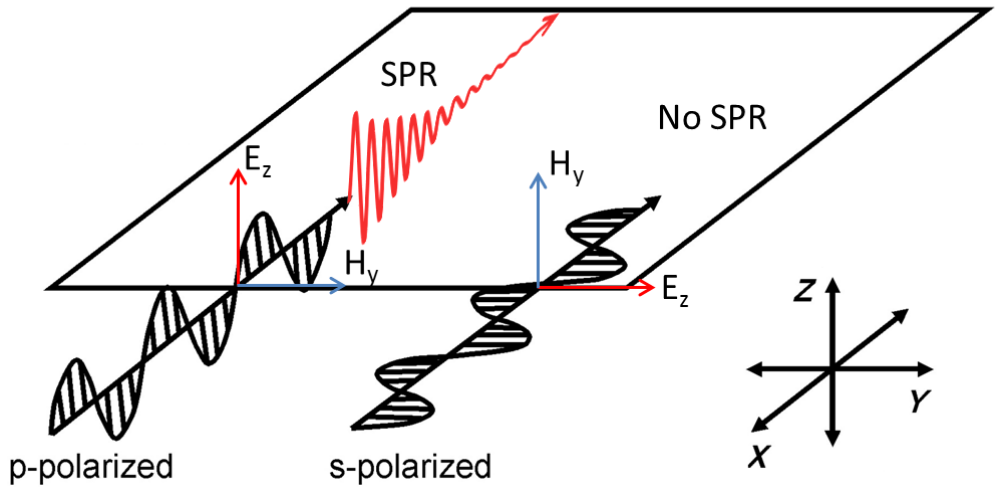

Figure 1.2 Coordinate system and directions for plasmon-coupled EM modes. P-polarized light, shown as electric field oscillations in z-direction, normal to interface (also called transverse magnetic due to magnetic field oscillating in the interfacial plane), excites SPR, which also has a z-direction oscillation in electron density. S-polarized light, with electric field oscillations in the interfacial plane (transverse electric), does not excite surface plasmons.

Materials in this report will be referred to by their dielectric constant (ε_i), having real (ε_i') and imaginary (ε_i'') parts as described by Equation 1.1,

$$\varepsilon_i = \varepsilon_i' + \varepsilon_i'' j \qquad \text{Equation 1.1}$$

as well as their complex refractive index (N_i), as described by Equation 1.2,

$$N_i = n_i + k_i j \qquad \text{Equation 1.2}$$

where n_i is the refractive index, k_i is the absorption constant, j is the imaginary unit, and i is an index, typically referring either to m for metal or d for dielectric. Material properties ε_i and N_i are equated with $\varepsilon_i = {N_i}^2$. Both ε_i and N_i are wavelength dependent, with well studied dispersive properties.[91]

Coupling a propagating EM wave to a surface bound mode is said to localize the EM wave to the surface.[90] This process of confining light to the surface of a metal-dielectric interface has been shown to increase the EM field by orders of magnitudes, as compared to the excitation field of freely propagating light.[90] This increased electromagnetic field and the sensitivity to refractive index (RI) within the field allows for the sensing utility discussed in the previous section.

In order to excite surface bound EM waves with light, the momentum of incident photons must match the momentum of the SP. When this matching occurs, energy carried by the photon transfers to SPs, which oscillate near the metal/dielectric interface as SPR. The physics and mathematics describing this coupling are derived from Maxwell's equations. While various treatments have been performed,[25,90] an abbreviated derivation is provided here.

Electromagnetic waves will be represented by vectors in the (x, y, z) space as shown in Figure 1.2 above. Also shown in that figure, only p-polarized (TM) light, light propagating

in the x-direction with electric field oscillations in the z-direction, and magnetic field oscillations in the y-direction, represented in vector form by $\vec{E} = (E_x, 0, E_z)$ in V/m and $\vec{H} = (0, H_y, 0)$ in A/m, can couple to SP modes. The resulting electromagnetic wave has the following form

$$\overrightarrow{A_1} = \overrightarrow{A_{10}}\exp(j(\overrightarrow{k_{x1}}\vec{x} + \overrightarrow{k_{z1}}\vec{z} - \omega t) \text{ in medium 1, z < 0} \qquad \text{Equation 1.3a}$$

and

$$\overrightarrow{A_2} = \overrightarrow{A_{20}}\exp(j(\overrightarrow{k_{x2}}\vec{x} - \overrightarrow{k_{z2}}\vec{z} - \omega t) \text{ in medium 2, z > 0} \qquad \text{Equation 1.3b}$$

where $\overrightarrow{A_i}$ stands for $\vec{E}$ or $\vec{H}$ in media i, $\overrightarrow{A_{io}}$ is the magnitude of the field, $\overrightarrow{k_x}$ is vector in the z-direction in inverse meters, ω is angular frequency in inverse seconds, and j is the imaginary unit. Both $\vec{E}$ and $\vec{H}$ fields must satisfy Maxwell's Equations:

$$\nabla \cdot \vec{H} = 0 \qquad \text{Equation 1.4}$$

$$\nabla \cdot \vec{E} = 0 \qquad \text{Equation 1.5}$$

$$\nabla \times \vec{E} + \frac{1}{c}\frac{\partial \vec{H}}{\partial t} = 0 \qquad \text{Equation 1.6}$$

$$\nabla \times \vec{H} - \frac{\varepsilon}{c}\frac{\partial \vec{E}}{\partial t} = 0 \qquad \text{Equation 1.7}$$

with c being the speed of light in a vacuum and ε is the dielectric constant of the material. These equations assume isotropic material properties, no charge, and no current through the materials.

At an interface, the tangential components of $\vec{E}$ and $\vec{H}$ fields must be equal. Thus,

$$E_{x1} = E_{x2} \qquad \text{Equation 1.8}$$

and

$$H_{y1} = H_{y2} \qquad \text{Equation 1.9}$$

From Equation 1.8, it follows immediately that $k_{x1} = k_{x2} = k_x$. This is saying that the momentum in the x-direction of the impinging light, must equal the momentum in the x-direction of the SP.

When Equation 1.3 is solved for in Equation 1.7, the resulting equations are

$$k_{z1}H_{y1} = \frac{\omega}{c}\varepsilon_1 E_{x1} \qquad \text{Equation 1.10}$$

and

$$k_{z2}H_{y2} = -\frac{\omega}{c}\varepsilon_2 E_{x2} \qquad \text{Equation 1.11}$$

When solving equations 10 and 11, the only nontrivial solution is

$$\frac{k_{z1}}{k_{z2}} = -\frac{\varepsilon_1}{\varepsilon_2} \qquad \text{Equation 1.12}$$

Equation 1.12 highlights the requirement for ε_d and ε_m, the dielectric functions of the two materials at the SPR interface, to be opposite in sign, as both k_{zi} components are positive. Most sensor applications are in media having positive $\varepsilon_1$values like air, gels or water (called ε_d for dielectric), the adjacent material must have a negative ε_2 value (called ε_m for metal) in the wavelength regime SPs are being excited. In the visible and near-visible regime, noble metals like Ag, Au, and Al are the most popular materials for SP excitation, as they fit the criteria. Each noble metal has unique dielectric properties as well as physical limitations, discussed in earlier and subsequent sections.

Continuing solving Maxwell's equations for the SP wave equations with appropriate boundary conditions, we get the following relationship for the wave vectors of in the SP in the dielectric

$$k_x{}^2 + k_{zd}{}^2 = \left(\frac{\omega}{c}\right)^2 \varepsilon_d \qquad \text{Equation 1.13}$$

or, rearranged we get

$$k_{zd} = \sqrt{\left(\frac{\omega}{c}\right)^2 \varepsilon_d - {k_x}^2} \qquad \text{Equation 1.14}$$

Substituting Equation 1.12 into 14 and using the known known frequency-wavelength relationship, $\frac{\omega}{c} = \frac{2\pi}{\lambda}$, we get the result of the Maxwell's equations for SPR as a dispersion relationship represented by

$$k_{SP} = k_x = \frac{2\pi}{\lambda}\sqrt{\frac{\varepsilon_d \varepsilon_m}{\varepsilon_d + \varepsilon_m}} \qquad \text{Equation 1.15}$$

which reveals several details about the SP wave vector. Since ε_m is a complex function (real and imaginary components as a function of wavelength or frequency), so is k_x, i.e. $k_x = k_x' + j * {k_x}''$. A nonzero imaginary part to the wave vector means there is a finite propagation length of the SP, defined by $l = \frac{1}{{k_x}''}$.

Next, in the spectral range of interest, because $\varepsilon_m < \varepsilon_d$ and $|\varepsilon_d| < |\varepsilon_m|$, we get that

$$\sqrt{\frac{\varepsilon_d \varepsilon_m}{\varepsilon_d + \varepsilon_m}} > \sqrt{\varepsilon_d} \qquad \text{Equation 1.16}$$

Results from this are several fold. First, substituting Equation 1.16 into 1.14, we see that k_{zd}, the wave vector of the SP in the dielectric, is purely imaginary. Substituting this into the wave vector equations, we see that this wave vector results in a bound, nonradiative mode that decays exponentially from a maximum value at the interface to zero as distance increases perpendicular to the interface. Incorporating this with the known wave vectors (propagating oscillatory wave along the surface with a propagation length of l), the surface plot shown in Figure 1.3 shows the field magnitude as a function along the x-axis and z-axis.[90]

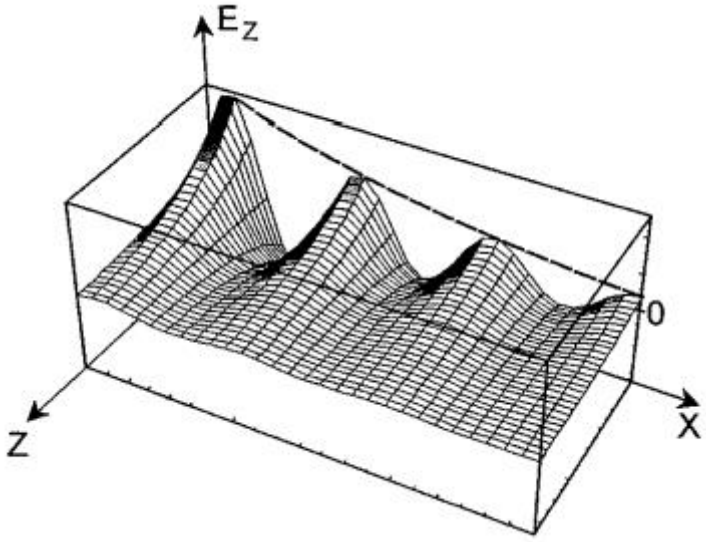

Figure 1.3 Surface plot of the evanescent and oscillatory characteristics of the surface bound mode excited at the metal dielectric interface in the xy-plane. The surface bound mode propagates as a damped oscillatory wave in the x-direction, while decaying exponentially in the z-direction.[90]

Another figure showing light impinging at an angle and coupling to surface bound modes is also shown in Figure 1.4. This figure also shows the damped oscillatory propagating mode in the x-direction and the evanescent wave in the z-direction.

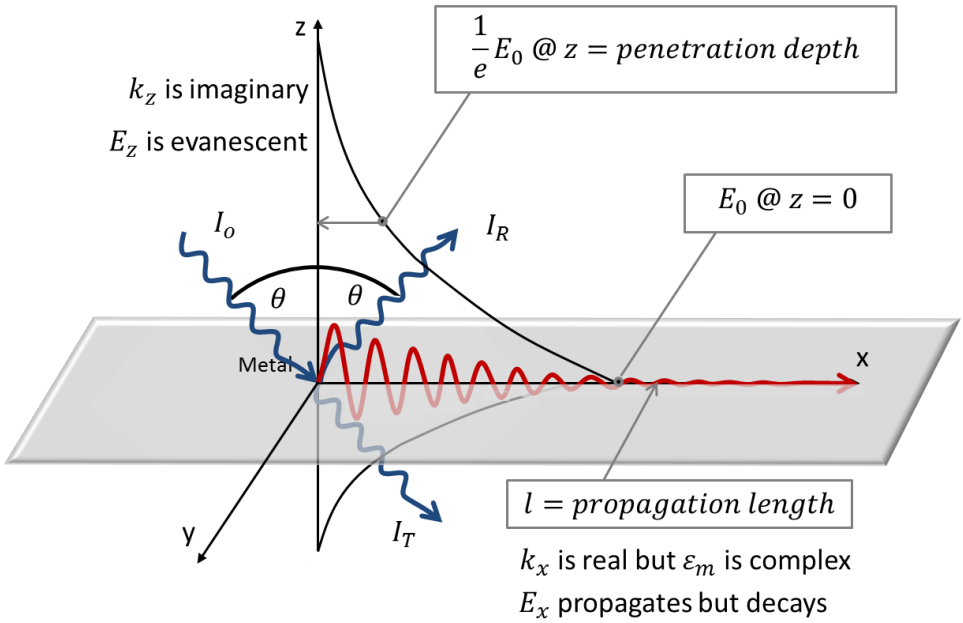

Figure 1.4 Impinging light waves coupling to a surface bound mode (SPR). Key components include impinging light (I_o), impingement angle (θ) with reference to normal, reflected light (I_R), transmitted light (I_T), wave vector in the x-direction (k_x), wave vector in the z-direction (k_z), electric field decay in the z-direction (E_z) due to evanescent wave form, and electric field decay in the x-direction (E_x) due to losses in the metal. The surface propagation is defined by the propagation length (l) and penetration depth ($\frac{1}{e}E_o$), where e is the base of the natural logarithm and E_o is the electric field intensity at the interface.

The second outcome of Equation 1.16 is that the momentum of a light propagating in a dielectric medium

$$k_{light} = \frac{2\pi}{\lambda}\sqrt{\varepsilon_d} \qquad \text{Equation 1.17}$$

is always smaller than the momentum of the surface plasmon. Furthermore, the wave vector of a surface plasmon is in the plane of the metal dielectric interface, so only the component of the light impinging in this direction will couple to the surface bound mode. This requires the inclusion of a $\sin\theta$ term, where θ is the angle of impingement with respect to normal (see light line equation inset in Figure 1.5).

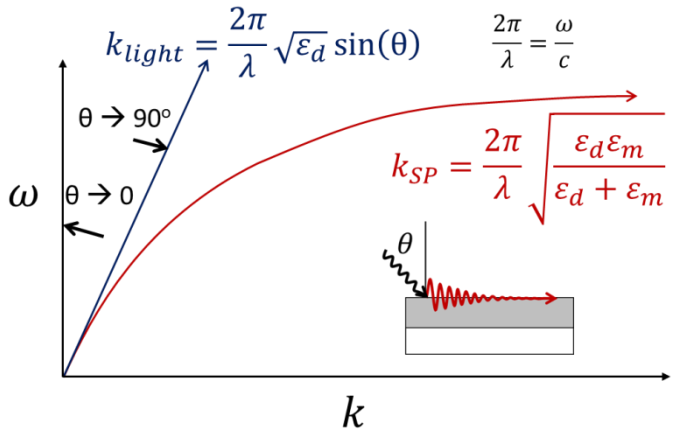

Figure 1.5 Wave vector of SPR and light in dielectric media. Note that the wave vector of light is never equal to that of the SP, thus matching never occurs. Furthermore, only the light in the plane of the SP propagation (xy-plane, with $\theta = 90°$) will couple to the SP mode.

The two prominent methods established to increase k_{light} to equal k_{SP} is prism coupling[9,11] and grating based coupling.[19,57] The wave vector of light for prism coupling is

$$k_{prism} = \frac{2\pi}{\lambda}\sqrt{\varepsilon_p}\sin\theta \qquad \text{Equation 1.18}$$

showing an increase in momentum due to an increased dielectric constant of the prism ε_p. The wave vector for diffracted light is

$$k_{gr} = k_{light,ll} + k_{diffraction} = \frac{2\pi}{\lambda}\sqrt{\varepsilon_d}\sin\theta + m\frac{2\pi}{\Lambda} \qquad \text{Equation 1.19}$$

Where m is the diffractive order and Λ is the periodicity of the grating.

Figure 1.6 shows the wave vectors if light and SP, with additional information about the two different coupling methods. The light line (shown as the solid blue line in Figure 1.6) is the wave vector of light (with a wavelength λ and frequency ω) propagating through a medium with a dielectric constant ε_d. When using a prism, the slope of the light line decreases (shown as the long dashed blue line labeled k_{prism} in Figure 1.6) allowing a prism to increase the wave vector of light due to the increased dielectric constant ε_p.

The remainder of the dashed blue lines in Figure 1.6 shows the increase in momentum from the grating diffraction term, where m are the diffractive order (top right inset in Figured 1.6) and Λ is the periodicity of the grating. Highlighted in this figure is the coupling frequencies from multiple diffractive orders.

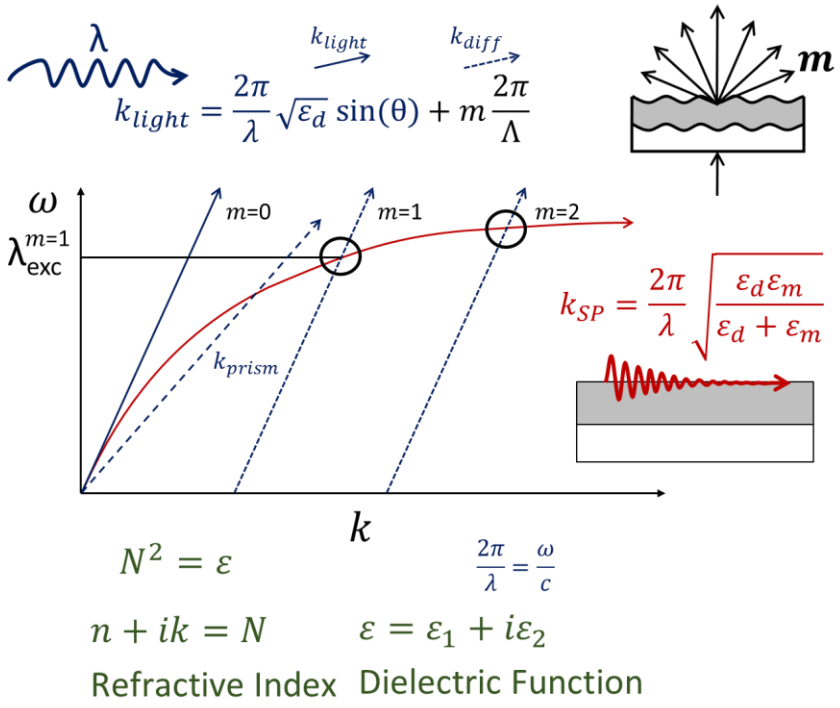

Figure 1.6 Surface plasmon, freely propagating light, diffracted light and light in a prism wave vectors plotted against frequencies. Insets show equations governing matching conditions as well as technical aspects about the coupling of propagating light waves to surface bound modes.

This completes the solving and analysis of the SP wave vector equations as coupled by freely propagating light. A summary is provided here, with a descriptive schematic in Figure 1.7. First, is a requirement for the impinging light to be polarized with the electric field oscillating perpendicular to the metal dielectric interface (p-polarized or TM). Next is an angle of impingement dependence, as only the component of light parallel to the metal-dielectric interface will couple a surface bound mode. Finally, the known characteristics of

propagating SPR modes are described through the previously solved equations: damped oscillatory propagation in x-direction with evanescent characteristic in the z-direction. These concepts and principles will be used in the following sections to apply grating based coupling to certain plasmonic application fields.

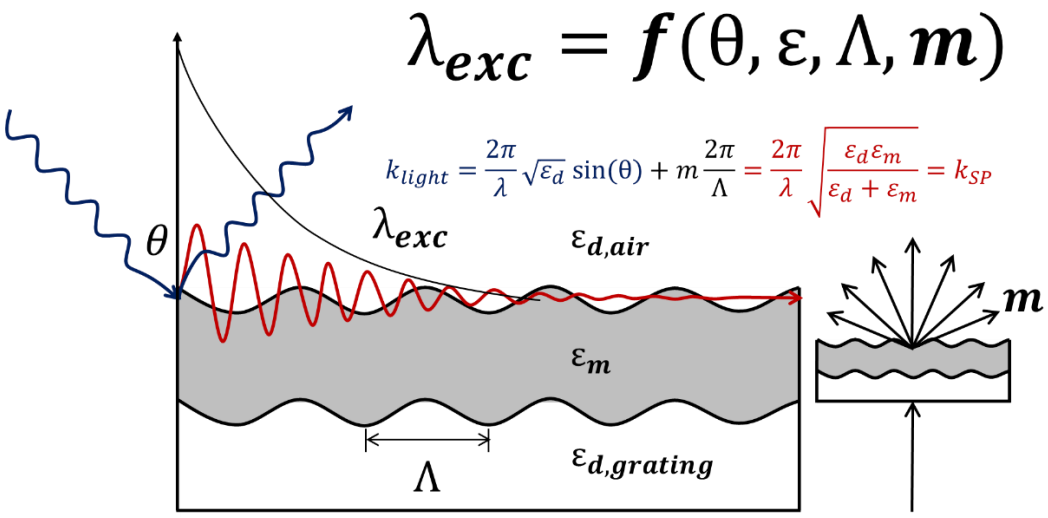

Figure 1.7 Summary of components of grating coupled-surface plasmon resonance (GC-SPR): Impinging light, impingement angle (θ), periodicity (Λ), diffractive order (m), dielectric constants (ε_i), and wavelength of excitation being a function of these variables.

1.3 Wave Vector Matching through Refractive Index Matching

The theory in the previous section considers single surface plasmon resonance modes. However, the existence of two surface plasmon (SP) modes when a metal film is thin (<50 nm) and surrounded by symmetric dielectric conditions had been theoretically and experimentally shown by 1960s.[92,93] These two modes are called symmetric and antisymmetric for their field distribution across the metal film.[93–95] These two modes are also referred to as long range surface plasmon resonance (LRSPR) and short range surface

plasmon resonance (SRSPR), due their vastly different penetration depths (referring to the decay length of the evanescent wave).

LRSPR is associated with a much larger penetration depth compared to normal SPR.[93] Traditional SPR has a small penetration depth, leading to difficulty for use in detecting large molecules and pathogens. However, LRSPR has been shown to be highly applicable in these larger analyte studies.[54,96] LRSPR has also been coupled with fluorescence[57] and hydrogel binding matrixes[54] to show increased sensitivity in small molecule studies. Long range surface plasmons have also been coupled to multiple resonance modes, leading to higher sensitivity, as shown in Figure 1.8.[97] As seen in this figure, and is the case with the other studies mentioned in this paragraph, prism based coupling is often used for these studies.

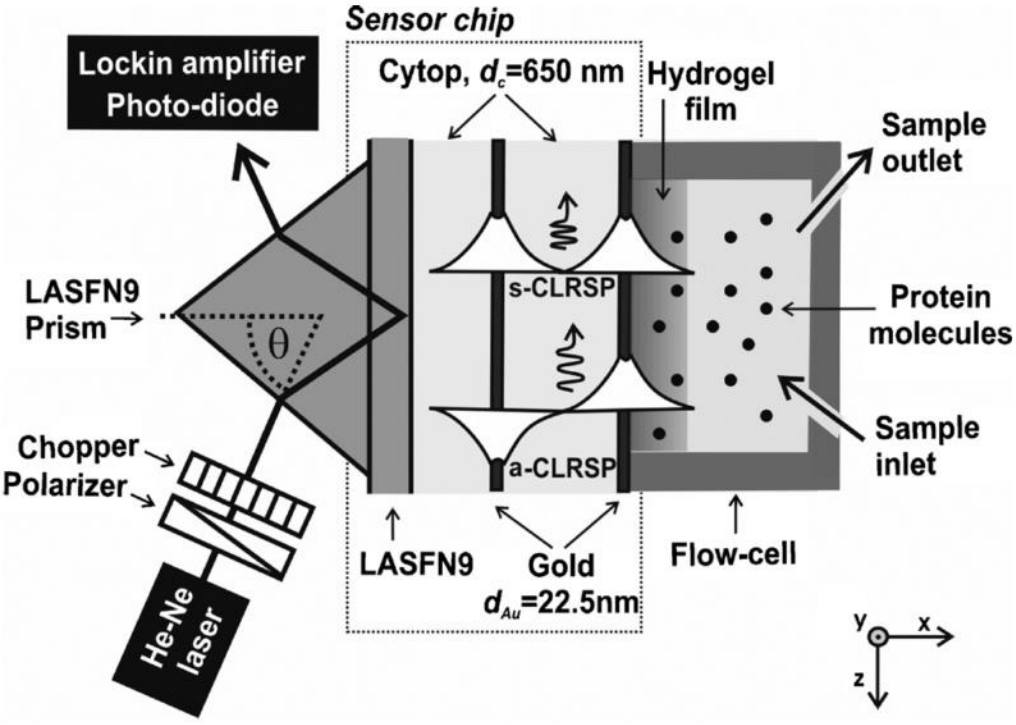

Figure 1.8 Example use of LRSPR to get higher sensitivity in analyte studies.[97]

There are several modes through which index matching can occur. First is submerging the thin metal film between a substrate of similar refractive indexes. This is a limiting scenario for classic polymers, but with the advent of index matching polymers (e.g. Teflon AF[43,98,99] and Cytop[54,55,59,96,97,100,101]), LRSPR has been demonstrated in aqueous solutions.

The system developed for this report involves the deposition of a high refractive index film on the ambient side of a thin metal film deposited on a grating. In this way, the addition of the high refractive index layer will shift the front side resonance location to match the back side resonance location, as shown in Figure 1.9. This will be the focus of Chapter 2 of this report.

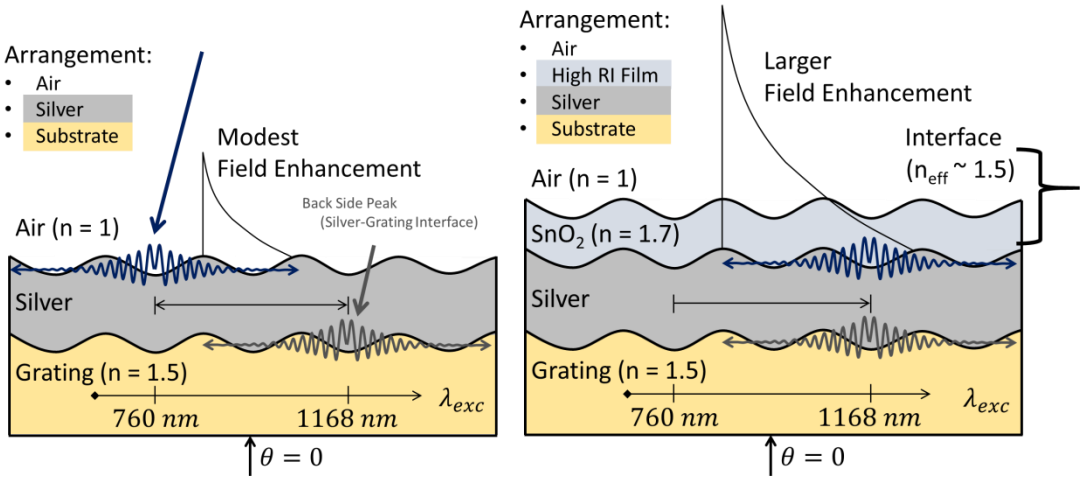

Figure 1.9 Shifting of the front side wave vector with deposition of front side high RI material

1.4 Fluorescence Enhancement

Fluorescence refers to the visible or near visible radiation of photons from a molecule resulting from excitation by an initial photon.[102,103] Primary research in the field of fluorescence involves imaging cells and tissues with microscopy[104–106] and detection, quantification, and characterization of molecules.[107,108] Among the diverse methods of advancing fluorescence studies, one way is to control the fluorescence decay lifetime is through the use of metals.[103,109] Recent advancements in plasmonics, a field exploiting the coupling of incident photons to electrons in a thin metal film, allow the fluorescence radiative decay process to be tuned through what is called metal enhanced fluorescence (MEF).[59,109–111] While the following focuses on MEF, it has been shown that the same principles apply to quantum dots (QDs).[73,112,113] It is claimed that QDs outperform organic fluorophores when used in conjunction with SPR due to increased scattering of colloidal QDs and due to QD photo stability compared to organic fluorophores which undergo bleaching.[73]

Metal enhanced fluorescence results through several modes.[58,109,111,114–117] First, the enhanced electric fields characteristic of surface plasmons (SPs) increases excitation light absorbed by the fluorophore.[109,111] This phenomenon will be referred to as surface plasmon enhanced absorption (SPEA). In general, metals enhance fluorescence by increasing radiative decay rates (Γ), resulting in a decreased decay lifetimes (τ) and increased quantum yields (Q).[109,111] It can be seen that (Figure 1.10) the smaller the initial quantum yield, the larger the potential for increasing the fluorescence yield. This reduced lifetime can allow normally low fluorescing molecules like DNA nucleotides to radiate an appreciable amount of fluorescence,[109] opening research space for varieties of new MEF characterization methods.

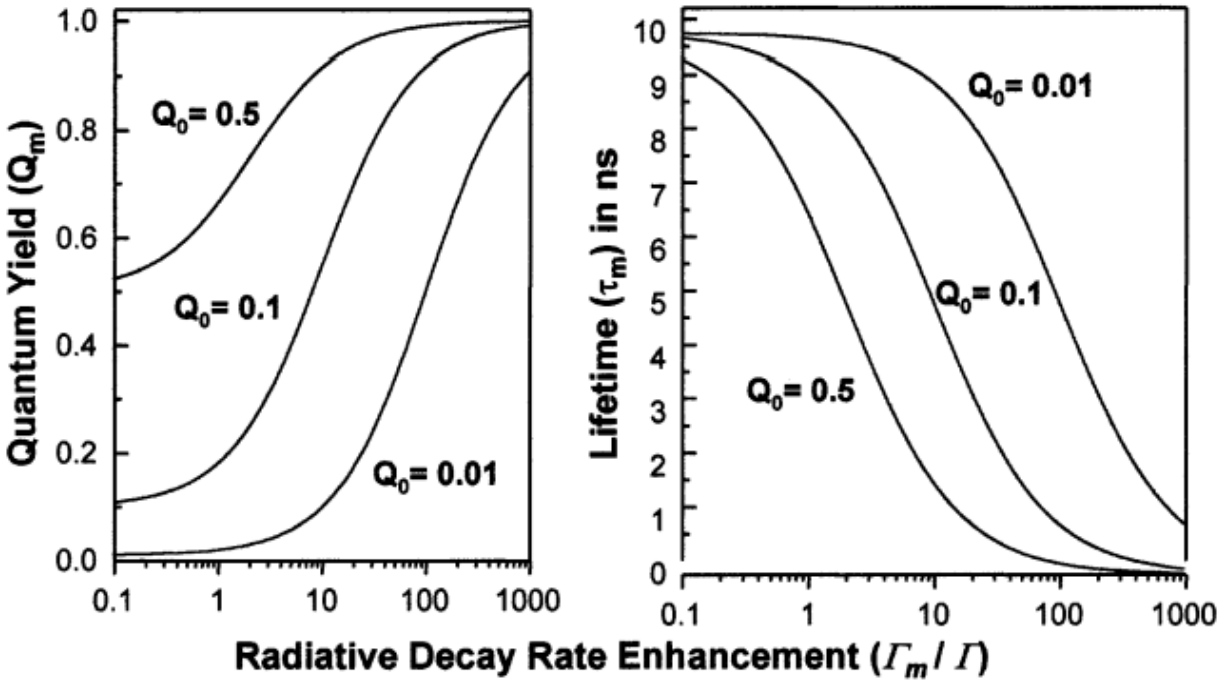

Figure 1.10 Change in quantum yield and lifetime with increase in radiative decay rate. Increases in decay rate can be achieved through the use of metal enhanced fluorescence. Subscript m denotes enhanced by metal.[109]

Metals also alter the relationships between fluorophores and quenchers, allowing for stronger and altered fluorescence spectra in the presence of quenchers.[109] Metal also allows for surface plasmon coupled emission (SPCE) which is directed, unlike the isotropic radiation from normal fluorophores.[58,63,113,116,118–122] Enhanced emission due to SPCE is polarized because the radiative plasmon modes emitting the light are p-polarized.[58,113,116,122]

Metal nanoparticles,[123,124] prisms with metal films[58,73] and nanostructured metal films[53,112,113,122,125,126] are typically used for MEF. Nanostructured films (referred to here as gratings) offer multiple, tunable diffractive modes dependent on the grating periodicity and angle/wavelength combination of incident light.[113] This tunability allows for gratings to utilize SPEA and SPCE individually or simultaneously depending on periodicity and impingement angle.[75] This broadens the use for fluorescence experiments.

This begins the discussion of technical considerations when designing MEF experiments. First, metals quench fluorescence through radiative energy transfer when within a small radius (typically <20 nm).[109,111] This means when fluorophores are too close to metal surfaces, the metal quenches the fluorescence, not allowing photon radiation. The goldilocks zone for MEF is typically between 20 to 200 nm from the metal surface. Fluorophores too far from the metal surface results in free space emission. The summary of this is shown below in Figure 1.11.

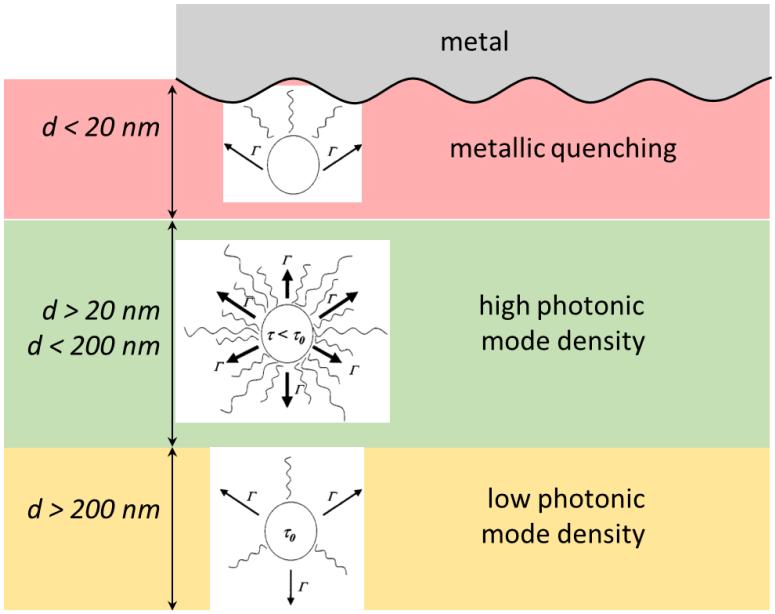

Figure 1.11 Metallic quenching and dynamic range of evanescent wave from surface plasmon means there is an optimal range (typically between 20 and 200 nm) for metal enhanced fluorescence.

Fluorophores can be immobilized near a metal surface in a variety of fashions. With appropriate surface chemistry and functionalization,[26,127,128] fluorophores can be directly linked to the metal surface through a variety of surface linkers commercially available. Some fluorophores can be dissolved into polymer precursors and subsequently spin coated onto grating substrates.[73,122] The optimum thickness depends on the specific fluorophore used and

grating geometry. Initial exploration of grating based MEF experiments spin-coated with a thin doped polymer will be the focus of Chapter 3 of this report.

1.5 References

(1) Wood, R. W. *Proc. Phys. Soc. London* **1902**, *18* (1), 269.
(2) Wood, R. W. *Philos. Mag. Ser. 6* **1912**, *23* (134), 310–317.
(3) Rayleigh, Lord. *Proc. R. Soc. London. Ser. A, Contain. Pap. a Math. Phys. Character* **1907**, *79* (532), 399–416.
(4) Hessel, A.; Oliner, A. A. *Appl. Opt.* **1965**, *4* (10), 1275.
(5) Ritchie, R. H. *Phys. Rev.* **1957**, *106* (5), 874–881.
(6) Powell, C. J.; Swan, J. B. *Phys. Rev.* **1960**, *118* (3), 640–643.
(7) Bohm, D.; Pines, D. *Phys. Rev.* **1951**, *82* (5), 625–634.
(8) Pines, D.; Bohm, D. *Phys. Rev.* **1952**, *85* (2), 338–353.
(9) Bohm, D.; Pines, D. *Phys. Rev.* **1953**, *92* (3), 609–625.
(10) Burstein, E. *J. Vac. Sci. Technol.* **1974**, *11* (6), 1004.
(11) Kretschmann, E.; Raether, H. *Zeitschrift Fuer Naturforschung, Tl. A* **1968**, *23* (November 1968), 2135.
(12) Kretschmann, E. *Zeitschrift für Phys.* **1971**, *241* (4), 313–324.
(13) Otto, A. *Zeitschrift für Phys.* **1968**, *216* (4), 398–410.
(14) Liedberg, B.; Nylander, C.; Lunström, I. *Sensors and Actuators* **1983**, *4*, 299–304.
(15) Pockrand, I.; Swalen, J. D.; Gordon, J. G.; Philpott, M. R. *Surf. Sci.* **1978**, *74* (1), 237–244.
(16) Peterlinz, K. A.; Georgiadis, R. *Opt. Commun.* **1996**, *130* (4-6), 260–266.
(17) Liedberg, B.; Lundström, I.; Stenberg, E. *Sensors Actuators B Chem.* **1993**, *11* (1-3), 63–72.
(18) Striebel, C.; Brecht, A.; Gauglitz, G. *Biosens. Bioelectron.* **1994**, *9* (2), 139–146.
(19) Cullen, D. C.; Brown, R. G. W.; Lowe, C. R.; Culle, D. C.; Brown, R. G. W.; Lowe, C. R. *Biosensors* **1987**, *3* (4), 211–225.
(20) Jory, M. J.; Bradberry, G. W.; Cann, P. S.; Sambles, J. R. *Meas. Sci. Technol.* **1995**, *6* (8), 1193.
(21) Lawrence, C. R.; Geddes, N. J.; Furlong, D. N.; Sambles, J. R. *Biosens. Bioelectron.* **1996**, *11* (4), 389–400.
(22) Moskovits, M. *Rev. Mod. Phys.* **1985**, *57* (3), 783–826.
(23) Willets, K. A.; Van Duyne, R. P. *Phys. Chem.* **2007**, *58*, 267–297.
(24) Haynes, C. L.; Van Duyne, R. P. *J. Phys. Chem. B* **2001**, *105* (24), 5599–5611.
(25) Homola, J.; Yee, S. S.; Gauglitz, G. *Sens. Actuators, B* **1999**, *54* (1–2), 3–15.
(26) Meneghello, A.; Antognoli, A.; Sonato, A.; Zacco, G.; Ruffato, G.; Cretaio, E.; Romanato, F. *Anal. Chem.* **2014**, *86* (23), 11773–11781.
(27) Yu, F.; Tian, S.; Yao, D.; Knoll, W. *Anal. Chem.* **2004**, *76* (13), 3530–3535.

(28) Silvestri, D.; Sonato, A.; Ruffato, G.; Meneghello, A.; Antognoli, A.; Cretaio, E.; Dettin, M.; Zamuner, A.; Casarin, E.; Zacco, G.; Romanato, F.; Morpurgo, M. *Anal. Methods* **2015**, *7* (10), 4173–4180.
(29) Singh, B. K.; Hillier, A. C. *Anal. Chem.* **2007**, *79* (14), 5124–5132.
(30) Wang, Y.; Brunsen, A.; Jonas, U.; Dostalek, J.; Knoll, W. *Anal. Chem.* **2009**, *81* (23), 9652.
(31) Zhu, H.; Snyder, M. *Curr. Opin. Chem. Biol.* **2003**, *7* (1), 55–63.
(32) Crespo-Biel, O.; Dordi, B.; Reinhoudt, D. N.; Huskens, J. *J. Am. Chem. Soc.* **2005**, *127* (20), 7594–7600.
(33) Jorgenson, R. C.; Yee, S. S. *Sens. Actuators, A* **1994**, *43* (1–3), 44–48.
(34) Mao, Y.; Bao, Y.; Wang, W.; Li, Z.; Li, F.; Niu, L. *Talanta* **2011**, *85* (4), 2106–2112.
(35) Pei, R. J.; Cui, X. Q.; Yang, X. R.; Wang, E. K. *Biomacromolecules* **2001**, *2* (2), 463–468.
(36) Petefish, J. W.; Hillier, A. C. *Anal. Chem.* **2014**, *86* (5), 2610–2617.
(37) Singh, B. K.; Hillier, A. C. *Anal. Chem.* **2006**, *78* (20), 7335–7340.
(38) Yeh, W.-H.; Hillier, A. C. *Anal. Chem.* **2013**, *85* (8), 4080–4086.
(39) Yeh, W.-H.; Petefish, J. W.; Hillier, A. C. *Anal. Chem.* **2011**, *83* (15), 6047–6053.
(40) Yeh, W.-H.; Petefish, J. W.; Hillier, A. C. *Anal. Chem.* **2012**, *84* (2), 1139–1145.
(41) Homola, J. *Anal. Bioanal. Chem.* **2003**, *377* (3), 528–539.
(42) Couture, M.; Zhao, S. S.; Masson, J.-F. *Phys. Chem. Chem. Phys.* **2013**, *15* (27), 11190–11216.
(43) Homola, J. J. *Chem. Rev.* **2008**, *108* (2), 462–493.
(44) Cooper, M. A. *Nature Reviews Drug Discovery*. 2002, pp 515–528.
(45) Myszka, D. G. *J. Mol. Recognit.* **1999**, *12* (5), 279–284.
(46) Huang, Y.-F.; Zhang, M.; Zhao, L.-B.; Feng, J.-M.; Wu, D.-Y.; Ren, B.; Tian, Z.-Q. *Angew. Chemie Int. Ed.* **2014**, *53* (9), 2353–2357.
(47) Lal, S.; Grady, N. K.; Kundu, J.; Levin, C. S.; Lassiter, J. B.; Halas, N. J. *Chem. Soc. Rev.* **2008**, *37* (5), 898–911.
(48) Nie, S.; Emory, S. R. *Science (80-.).* **1997**, *275* (5303), 1102–1106.
(49) Campion, A.; Kambhampati, P.; Campion, A.; Kambhampati, P. *Chem. Soc. Rev.* **1998**, *27* (4), 241–250.
(50) Zhou, F.; Liu, Y.; Cai, W. *Opt. Lett.* **2014**, *39* (5), 1302–1305.
(51) Miyake, H.; Ye, S.; Osawa, M. *Electrochem. Commun.* **2002**, *4* (12), 973–977.
(52) Le, F.; Brandl, D. W.; Urzhumov, Y. A.; Wang, H.; Kundu, J.; Halas, N. J.; Aizpurua, J.; Nordlander, P. *ACS Nano* **2008**, *2* (4), 707–718.
(53) Smolyaninov, I. I.; Hung, Y. J.; Davis, C. C. *Conf. Quantum Electron. Laser Sci. - Tech. Dig. Ser.* **2007**, *14* (22), 10825–10830.
(54) Huang, C.-J.; Dostalek, J.; Sessitsch, A.; Knoll, W. *Anal. Chem.* **2011**, *83* (3), 674–677.
(55) Chun Jen, H.; Jakub, D.; Wolfgang, K. *J. Vac. Sci. Technol., B Microelectron. Nanom. Struct.* **2010**, *28*, 66.
(56) Ekgasit, S.; Thammacharoen, C.; Yu, F.; Knoll, W. *Anal. Chem.* **2004**, *76* (8), 2210–2219.
(57) Kasry, A.; Knoll, W. *Appl. Phys. Lett.* **2006**, *89* (10), 101103–101106.
(58) Lakowicz, J. R. *Anal. Biochem.* **2004**, *324* (2), 153–169.

(59) Bauch, M.; Toma, K.; Toma, M.; Zhang, Q.; Dostalek, J. *Plasmonics* **2014**, *9* (4), 781–799.
(60) Lakowicz, J. R.; Ray, K.; Chowdhury, M.; Szmacinski, H.; Fu, Y.; Zhang, J.; Nowaczyk, K. *Analyst* **2008**, *133* (10), 1308.
(61) Ekgasit, S.; Yu, F.; Knoll, W.; Biosensor, S. *Langmuir* **2005**, *21* (9), 4077–4082.
(62) Hecht, B.; Sick, B.; Wild, U. P.; Deckert, V.; Zenobi, R.; Martin, O. J. F.; Pohl, D. W. *J. Chem. Phys.* **2000**, *112* (18), 7761–7774.
(63) Qiu, D.; Zhang, D.; Chen, Y.; Zhu, L.; Han, L.; Wang, P.; Ming, H.; Badugu, R.; Lakowicz, J. R. *Opt. Lett.* **2014**, *39* (15), 4341–4344.
(64) Beck, F. J.; Polman, A.; Catchpole, K. R. *J. Appl. Phys.* **2009**, *105* (11), 114310–114317.
(65) Kamat, P. V. *J. Phys. Chem. C* **2007**, *111* (7), 2834–2860.
(66) Linic, S.; Christopher, P.; Ingram, D. B. *Nat Mater* **2011**, *10* (12), 911–921.
(67) Pillai, S.; Catchpole, K. R.; Trupke, T.; Green, M. A. *J. Appl. Phys.* **2007**, *101* (9), 93105–93108.
(68) Yoon, W.-J.; Jung, K.-Y.; Liu, J.; Duraisamy, T.; Revur, R.; Teixeira, F. L.; Sengupta, S.; Berger, P. R. *Sol. Energy Mater. Sol. Cells* **2010**, *94* (2), 128–132.
(69) West, P. R.; Ishii, S.; Naik, G. V.; Emani, N. K.; Shalaev, V. M.; Boltasseva, A. *Laser Photonics Rev.* **2010**, *4* (6), 795–808.
(70) Kretschmann, E. *Opt. Commun.* **1972**, *5* (5), 331–336.
(71) Ritchie, R. H. *Phys. status solidi* **1970**, *39* (1), 297–308.
(72) Nagpal, P.; Lindquist, N. C.; Oh, S.-H.; Norris, D. J. *Science (80-.).* **2009**, *325* (5940), 594–597.
(73) Gryczynski, I.; Malicka, J.; Jiang, W.; Fischer, H.; Chan, W. C. W.; Gryczynski, Z.; Grudzinski, W.; Lakowicz, J. R. *J. Phys. Chem. B* **2005**, *109* (1), 1088–1093.
(74) Abbas, A.; Linman, M.; Cheng, Q. *Biosens. Bioelectron.* **2011**, *26* (5), 1815–1824.
(75) Kaplan, B.; Guner, H.; Senlik, O.; Gurel, K.; Bayindir, M.; Dana, A. *Plasmonics* **2009**, *4* (3), 237–243.
(76) Giannattasio, A.; Barnes, W. *Opt. Express* **2005**, *13* (2), 428–434.
(77) Magnusson, R.; Svavarsson, H. G.; Yoon, J.; Shokooh-Saremi, M.; Song, S. H. *Appl. Phys. Lett.* **2013**, *100* (9), 091106.
(78) Chang, S.-H.; Gray, S.; Schatz, G. *Opt. Express* **2005**, *13* (8), 3150–3165.
(79) Halpern, A. R.; Corn, R. M. *ACS Nano* **2013**, *7* (2), 1755–1762.
(80) Lindquist, N. C.; Nagpal, P.; Lesuffleur, A.; Norris, D. J.; Oh, S.-H. *Nano Lett.* **2010**, *10* (4), 1369–1373.
(81) Chung, A. J.; Huh, Y. S.; Erickson, D. *Nanoscale* **2011**, *3* (7), 2903–2908.
(82) Wang, S.; Pile, D. F. P.; Sun, C.; Zhang, X. *Nano Lett.* **2007**, *7* (4), 1076–1080.
(83) Franzen, S. *J. Phys. Chem. C* **2008**, *112* (15), 6027–6032.
(84) Chiu, N.-F.; Lin, C.; Lee, J.-H.; Kuan, C.; Wu, K.; Lee, C.; Yu, C.; Nien, S.-Y.; Lee, J.-H.; Kuan, C.; Wu, K.; Lee, C.; Lin, C.; Nan-Fu, C.; Chii-Wann, L.; Jiun-Haw, L.; Chieh-Hsiung, K.; Kuang-Chong, W.; Chih-Kung, L. *Appl. Phys. Lett.* **2007**, *91* (8), 83114.
(85) Petefish, J. **2014**.
(86) Chegel, V.; Whitcombe, M. J.; Turner, N. W.; Piletsky, S. A. *Biosens. Bioelectron.* **2009**, *24* (5), 1270–1275.
(87) Moharam, M. G.; Gaylord, T. K. *J. Opt. Soc. Am. A* **1986**, *3* (11), 1780–1787.

(88) Moharam, M. G.; Grann, E.; Pommet, D.; Gaylord, T. K. *J. Opt. Soc. Am. A* **1995**, *12* (5), 1068–1076.
(89) Moharam, M. G.; Pommet, D.; Grann, E.; Gaylord, T. K. *J. Opt. Soc. Am. A* **1995**, *12* (5), 1077–1086.
(90) Knoll, W. *Annu. Rev. Phys. Chem.* **1998**, *49* (1), 569–638.
(91) MAIER, S. A. *Plasmonics: Fundamentals and Applications*; Springer: 233 Spring Street, New York, NY 10013, USA, 2007; Vol. 1.
(92) Boersch, H.; Geiger, J.; Imbusch, A.; Niedrig, N. *Phys. Lett.* **1966**, *22* (2), 146–147.
(93) Sarid, D. *Phys. Rev. Lett.* **1981**, *47* (26), 1927–1930.
(94) Stegeman, G. I.; Burke, J. J.; Hall, D. G. *Opt. Lett.* **1983**, *8* (7), 383.
(95) Burke, J. J.; Stegeman, G. I.; Tamir, T. *Phys. Rev. B* **1986**, *33* (8), 5186–5201.
(96) Wang, Y.; Knoll, W.; Dostalek, J. *Anal. Chem.* **2012**, *84* (19), 8345–8350.
(97) Dostálek, J.; Roskamp, R. F.; Knoll, W. *Sensors Actuators B Chem.* **2009**, *139* (1), 9–12.
(98) Nenninger, G. G.; Tobiška, P.; Homola, J.; Yee, S. S. *Sens. Actuators, B* **2001**, *74* (1–3), 145–151.
(99) Dostálek, J.; Kasry, A.; Knoll, W. *Plasmonics* **2007**, *2* (3), 97–106.
(100) Joo, Y. H.; Song, S. H.; Magnusson, R. *Opt. Express* **2009**, *17* (13), 10606.
(101) Huang, C. J.; Dostalek, J.; Knoll, W. *Biosens. Bioelectron.* **2010**, *26* (4), 1425–1431.
(102) Ishikawa-Ankerhold, H. C.; Ankerhold, R.; Drummen, G. *Molecules*. 2012, pp 4047–4132.
(103) Noomnarm, U.; Clegg, R. *Off. J. Int. Soc. Photosynth. Res.* **2009**, *101* (2), 181–194.
(104) *Curr. Biol.* **1994**, *4* (5), 443.
(105) Yang, T.-T.; Kain, S. R.; Kitts, P.; Kondepudi, A.; Yang, M. M.; Youvan, D. C. *Gene* **1996**, *173* (1), 19–23.
(106) Chen, W.; Long, K. D.; Yu, H.; Tan, Y.; Choi, J. S.; Harley, B. a; Cunningham, B. T. *Analyst* **2014**, *139* (22), 5954–5963.
(107) Basché, T. *J. Lumin.* **1998**, *76-77*, 263–269.
(108) Patterson, G. H. *Semin. Cell Dev. Biol.* **2009**, *20* (8), 886–893.
(109) Geddes, C. D.; Lakowicz, J. R. *J. Fluoresc.* **2002**, *12* (2), 121–129.
(110) Szmacinski, H.; Lakowicz, J. R. *Anal. Chem.* **2008**, *80* (16), 6260–6266.
(111) Liebermann, T.; Knoll, W. *Colloids Surf., A* **2000**, *171* (1–3), 115–130.
(112) Kim, K.; Kim, D. J.; Kim, D. *Quantum Dots, Part. Nanoclusters Vi* **2009**, *7224*, SPIE.
(113) Hao, Y.; Wang, H.; Zhang, Z.; Zhang, X. L.; Chen, Q.; Sun, H. *J. Phys. Chem. C* **2013**, *117* (50), 26734–26739.
(114) Neumann, T.; Johansson, M.-L.; Kambhampati, D.; Knoll, W. *Adv. Funct. Mater.* **2002**, *12* (9), 575–586.
(115) Lakowicz, J. R.; Shen, Y.; D'Auria, S.; Malicka, J.; Fang, J.; Gryczynski, Z.; Gryczynski, I. *Anal. Biochem.* **2002**, *301* (2), 261–277.
(116) Gryczynski, I.; Malicka, J.; Gryczynski, Z.; Lakowicz, J. R. *Anal. Biochem.* **2004**, *324* (2), 170–182.
(117) Lakowicz, J. R. *Anal. Biochem.* **2005**, *337* (2), 171–194.
(118) Gryczynski, I.; Malicka, J.; Gryczynski, Z.; Lakowicz, J. R. *J. Phys. Chem. B* **2004**, *108* (33), 12568–12574.
(119) Wedge, S.; Wasey, J. a E.; Barnes, W. L.; Sage, I. *Appl. Phys. Lett.* **2004**, *85* (2004), 182–184.

(120) Andrew, P.; Barnes, W. L. *Science* **2004**, *306* (5698), 1002–1005.
(121) Cao, S.-H.; Cai, W.-P.; Liu, Q.; Li, Y.-Q. *Annu. Rev. Anal. Chem.* **2012**, *5* (1), 317–336.
(122) Zhang, Z. Z.; Wang, H. H.; Du, J. J.; Zhang, X. L.; Hao, Y. Y.; Chen, Q.; Sun, H. *IEEE Photonics Technol. Lett.* **2015**, *27* (8), 821–823.
(123) Cheng, Z.; Li, G.; Liu, M. *Sensors Actuators B Chem.* **2015**, *212*, 495–504.
(124) Chen, J.; Wang, K.; Wu, K.; Qian, L.; Long, H.; Wang, B.; Lu, P. *Opt. Commun.* **2015**, *349*, 180–184.
(125) Bhatnagar, K.; Pathak, a; Menke, D.; Cornish, P. V; Gangopadhyay, K.; Korampally, V.; Gangopadhyay, S. *Nanotechnology* **2012**, *23* (49), 495201.
(126) Miomandre, F.; Audibert, J. F.; Zhou, Q.; Audebert, P.; Martin, P.; Lacroix, J. C. *Electrochim. Acta* **2013**, *110*, 56–62.
(127) Tawa, K.; Hori, H.; Kintaka, K.; Kiyosue, K.; Tatsu, Y.; Nishii, J. *Opt. Express* **2008**, *16* (13), 9781–9790.
(128) Pokhriyal, A.; Lu, M.; Chaudhery, V.; Huang, C.-S.; Schulz, S.; Cunningham, B. T. *Opt. Express* **2010**, *18* (24), 24793–24808.
(129) Ekgasit, S.; Tangcharoenbumrungsuk, A.; Yu, F.; Baba, A.; Knoll, W. *Sens. Actuators, B* **2005**, *105* (2), 532–541.
(130) Toma, K.; Vala, M.; Adam, P.; Homola, J.; Knoll, W.; Dostálek, J. *Opt. Express* **2013**, *21* (8), 10121.
(131) White, I. M.; Fan, X. *Opt. Express* **2008**, *16* (2), 1020–1028.
(132) Homola, J.; Koudela, I.; Yee, S. S. *Sens. Actuators, B* **1999**, *54* (1–2), 16–24.
(133) Cui, X.; Tawa, K.; Hori, H.; Nishii, J. *Appl. Phys. Lett.* **2009**, *95* (13), 133117.
(134) Devaux, E.; Ebbesen, T. W.; Weeber, J. C.; Dereux, A. *Appl. Phys. Lett.* **2003**, *83* (24), 4936–4938.
(135) Barnes, W. L.; Dereux, A.; Ebbesen, T. W. *Nature* **2003**, *424* (6950), 824.
(136) Ekgasit, S.; Thammacharoen, C.; Knoll, W. *Anal. Chem.* **2004**, *76* (3), 561–568.
(137) Gupta, G.; Kondoh, J. *Sens. Actuators, B* **2007**, *122* (2), 381–388.
(138) Cai, D. B.; Lu, Y. H.; Lin, K. Q.; Wang, P.; Ming, H. *Opt. Express* **2008**, *16* (19), 14597–14602.
(139) Mu, W.; Buchholz, D. B.; Sukharev, M.; Jang, J. I.; Chang, R. P. H.; Ketterson, J. B. *Opt. Lett.* **2010**, *35* (4), 550.
(140) Singh, B. K.; Hillier, A. C. *Anal. Chem.* **2008**, *80* (10), 3803–3810.
(141) Chandezon, J.; Dupuis, M. T.; Cornet, G.; Maystre, D. *J. Opt. Soc. Am.* **1982**, *72* (7), 839–846.
(142) Dostálek, J.; Homola, J.; Miler, M. *Sensors Actuators B Chem.* **2005**, *107* (1), 154–161.
(143) Leveque, G.; Martin, O. J. F. *J. Appl. Phys.* **2006**, *100* (12), 6.
(144) Li, S.-Q.; Guo, P.; Buchholz, D. B.; Zhou, W.; Hua, Y.; Odom, T. W.; Ketterson, J. B.; Ocola, L. E.; Sakoda, K.; Chang, R. P. H. *ACS Photonics* **2014**, *1* (3), 163–172.
(145) Ekgasit, S.; Yu, F.; Knoll, W. *Sens. Actuators, B* **2005**, *104* (2), 294–301.
(146) Estevez, M. C.; Otte, M. A.; Sepulveda, B.; Lechuga, L. M. *Anal. Chim. Acta* **2014**, *806*, 55–73.
(147) Quail, J. C.; Rako, J. G.; Simon, H. J. *Opt. Lett.* **1983**, *8* (7), 377–379.
(148) Palik, E. D. *J. Opt. Soc. Am. A* **1984**, *1* (12), 1297.
(149) Yeh, W. **2013**.

CHAPTER 2

HIGH REFRACTIVE INDEX SURFACE PLASMON WAVE VECTOR MATCHING ACROSS A THIN METAL FILM GRATING PROBED WITH REFRACTIVE INDEX SENSING

2.1 Abstract

Investigations in grating coupled surface plasmon resonance often use only single mode resonances. In this study, we demonstrate the coupling of distinct surface plasmon resonance modes on opposite sides of a metal-coated grating through deposition of a submicron, high refractive index ambient layer. This coupling occurs by matching the resonance wavelengths, a function of the optical properties, across the metal-dielectric interface. The high refractive index coating creates an effective matching of optical properties across the metal film, shifting the resonance condition of the ambient plasmon wave vector, allowing it to couple and enhance with the substrate side wave vector. In this work, gratings were coated with a semi-transparent layer (~50 nm) of silver, followed by a dielectric coating of tin oxide at various thicknesses. Over an order of magnitude increase in transmission enhancement is shown, from 5-fold transmission enhancement through a bare silver grating referenced with flat silver to 100-fold enhancement after deposition of a tin oxide layer of appropriate thickness (~300 nm). Using a combination of angle-dependent optical dispersion measurements (Supporting Information) and numerical modeling for films of various thickness, we are able to demonstrate the evolution of plasmon modes from an unmatched to matched condition, where they couple to provide extraordinary optical transmission enhancement. This optical transmission enhancement is then probed through

analytical experiments with liquids of various refractive indexes and computational studies. This system shows a change in sensing variable from wavelength tracking in bare silver to intensity tracking with the matched system.

2.2 Introduction

Surface plasmon resonance (SPR) is a powerful and highly versatile optical phenomena utilized for various analytical measurements such as label free sensing of adsorption,[99] measurement of binding affinities,[19,41,42] and monitoring thin film deposition.[32,35,38,39] These measurements exploit SPR's sensitivity to changes in surface optical properties,[25,90] namely deviations in near-field optical parameters such as refractive index. The enhanced surface electric field associated with SPR can also be used to enhance or amplify surface spectroscopies. Examples of this include Surface Enhanced Raman Spectroscopy (SERS),[23,47,49,52] Surface Enhanced Infrared Absorption (SEIRA),[23,36,47,51,52] and SPR enhanced fluorescent spectroscopy.[99,125,129,130]

The suitability of SPR for specific applications is related to the localization and wavelength dependence of the electric field enhancement.[42,74,131] Factors affecting this field enhancement include the plasmon coupling method (e.g., prism, grating, waveguide),[25,131,132] surface topology,[42,75,76,133–135] layer composition and thickness,[33,39,61,98,99,136] and incident light angle and wavelength.[43,98,137] Both prism and grating coupled SPR sensors have high sensitivity for binding studies.[132,138] However, both have drawbacks. Spectral location and angle of the SPR peak is limited by the prism refractive index (RI).[137] While generally less sensitive for RI sensing, nanostructured surfaces, such as gratings, offer tunability through manipulation of the angle of incidence and length scale of the surface periodicity.[39,75] They

also provide increased information density by plasmon excitation through multiple diffractive orders.[38,39,70,87,139–142]

Factors affecting the plasmonic response of nanostructured surfaces include the amplitude, shape and periodicity of the surface profile.[75,76,143] Degrees of grating symmetry also affect plasmonic responses, as 2D gratings excite surface plasmons (SPs) differently and can increase sensitivity.[42,79,122,144] With such a breadth of variables available for manipulation, plasmonic systems can be tuned and optimized for a variety of needs, whether the device is acting as a biosensor[19,41,54,99,101,145,146] or used to couple to molecular processes such as fluorescence emission[56,99,111,130] or vibrational modes.[36,37,40,47,49,52]

Studies done on prisms with thin metal films and metallic gratings typically exploit a single plasmon mode, typically performed in reflection configuration[15,36,39]. This single resonance is simple and clean, and with no light transmission, one knows how reflected and absorbed light is related. However, thin layers of metal (0-100 nm) on a diffraction grating are capable of exciting two plasmon modes, on either side of the metal film, allowing for larger optical responses, greater field localization and use of both plasmon modes for different spectroscopic needs.[43]

If the optical properties across the thin metal film are unmatched, as in the example of substrate and ambient condition of different optical properties, two SP modes will occur according to the wave vector matching equation (Equation 15 from Chapter 1). In this unmatched system, the two relevant interfaces are substrate/silver and the silver/ambient interfaces. It has been shown previously that in this unmatched configuration there are two distinct plasmon modes occurring on either side of the silver film.[39,140]

Despite its utility, single resonance modes can be fundamentally altered and enhanced with the involvement on subsequent resonance modes. For example, if one wants to use SPR to enhance a spectroscopic process, then larger electric field localization due to a larger SPR would be preferred.[101,111,145] This can be accomplished by coupling of front and back side resonant conditions across a metal film by matching the optical properties across the silver film, providing long range and short range surface plasmon resonance (LRSPR and SRSPR, respectively).[43,147]

A demonstrated method for matching wave vectors is to create symmetry by sandwiching a thin metal film between dielectric layers of matching refractive index.[84,98] For example, for aqueous applications, an index-matching layer possessing a refractive index similar to water (e.g., Cytop, Teflon AF)[96,98,99,101] can be coated under the metal film to create optical symmetry with the opposing water interface. This technique has been used to create matching conditions in both prism and grating based applications and has resulted in substantially improved detection limits.[96,98,99] Drawbacks to index-matching polymers include the high cost of materials and experimental limitations, including the system only functioning in aqueous environments (i.e. symmetry does not exist in air phase sensing).

To address these drawbacks, while still providing the benefits of LRSPR, we have pursued a robust index matching method involving the coating of a high RI film onto the ambient side of a metal-coated grating.

In this work, we describe a method for index matching in a grating-coupled SPR system that exploits a submicron layer of a high refractive index material composed of tin oxide (SnO_2) coated on a silver-coated grating. Tin oxide films of various thicknesses are deposited

directly onto a silver-coated grating using reactive DC sputtering of a tin target in an oxygen atmosphere.

2.3 Experimental Section

2.3.1 Materials

Silver wire (99.995% purity) and tungsten wire baskets for evaporation were acquired from Ted Pella (Redding, CA). The tin sputtering target (99.99% purity) was purchased from AJA International (North Scituate, MA). The UV curable polymer (NOA 61, Norland, Cranbury, NJ) and polydimethylsiloxane silicone elastomer kit (SYLGARD 184, Dow Corning, Midland, MI) were used as received. Recordable digital versatile discs (MAM-A 16X Silver DVD-R) were from MAM-A (Colorado Springs, Colorado).

2.3.2 Grating Fabrication

Commercial DVD-Rs were split with a razor blade, cleaned, and replicated onto clean glass slides with a UV curable polymer, as described in previous publications.[38,140] Gratings were subsequently coated via thermal evaporation with ~50 nm of silver, as monitored by a quartz crystal thickness monitor. Tin oxide was then deposited onto the silver through reactive DC sputtering (ATC 1800, AJA International) of a tin target in a partial oxygen environment. Typical conditions were 30 SCCM (standard cubic centimeters per minute) argon and 25 SCCM oxygen, yielding a chamber pressure of around 7 mTorr. The sputter power was set to 75 W, with typical voltage and current ranging between 345-360 V and 206-220 mA, respectively. Tin oxide layers were deposited to produce films with thicknesses

ranging between 25-400 nm. The deposition stage rotated at 30 RPM to increase film uniformity. Figure 1 depicts the details of the grating and film layers.

2.3.3 Ellipsometry

The various films were analyzed for thickness and optical quality with spectroscopic ellipsometry at wavelengths between 380 and 900 nm and at angles of incidence of 65°, 70° and 75° (Alpha-SE, J.A. Woollam Co., Lincoln, NE). Numerical modeling was used to obtain film thickness and refractive index values of the various films by fitting a multilayer reflectance model to the measured Delta and Psi ellipsometry parameters (see Supporting Information 2.7.2 for details).

2.3.4 Optical Characterization

Transmission spectra were measured with a custom-built variable angle optical train as described previously.[38,140] White light from a broadband halogen source (OSL1, Thorlabs Inc, New Jersey, USA) was collimated using a convex lens with a focal length of 150 mm (Newport Optics). The collimated beam passed through a Glan Thompson polarizer followed by a variable diameter aperture (typically held between 0.5 to 1 cm depending on amount of light required). The resulting beam impinged on the sample mounted to a motorized rotation stage. The transmitted light was collected with a 600 μm, bifurcated optical fiber that sent the light to two different spectrometers. The first measured spectral intensity at wavelengths between 350-1000 nm (HR400CG, Ocean Optics) while the second measured between 800-2500 nm (NIRQuest512-2.5, Ocean Optics). Results from both spectrometers were combined to create a composite signal between 350 and 2500 nm. Normal incidence spectra were

collected with incident light perpendicular to the sample surface ($\theta = 0°$). All spectra were referenced to light transmitted through a flat silver on glass film of the same thickness at normal impingement ($\theta = 0°$).

2.3.5 Refractive Index Sensing

Various liquids were used to change the bulk refractive index to probe the sensitivity of the unmatched (bare silver) and matched (high RI on silver) plasmonic sensors. The three liquids used were 100% DIW, 50% DIW-50% glycerol, and 100% glycerol, with a bulk refractive index of 1.33, 1.4, and 1.475, respectively. A glass cover slip was used to decrease aberrations from the curvature of the liquid drop on. The normal incidence transmission setup was used to collect spectra using both spectrometers, as described in 2.3.4.

2.3.6 Optical Modeling

Predictions of the optical transmission results were computed using a custom MatLab protocol that used the rigorously-couple wave analysis (RCWA) method to solve for the optical response of the grating geometry.[87–89] This protocol computed transmission and reflection efficiencies using both transverse magnetic (TM) and transverse electric (TE) incident light as a function of wavelength and angle of incidence (see Supporting Information 2.7.3 for more details).

2.4 Results and Discussion

2.4.1 Orientation to Results: Fabrication and Optical Experiments

When solving the wave vector matching equation for wavelength of excitation, the following equation is found[43,90]:

$$\lambda = \frac{\Lambda}{m}\left(\pm Re\sqrt{\frac{\varepsilon_d \varepsilon_m}{\varepsilon_d + \varepsilon_m}} + \sqrt{\varepsilon_d}\sin\theta\right) \qquad \text{Equation 2.1}$$

This equation shows that the spectral location (wavelength λ) of the matching condition for diffracted light is a function of the grating periodicity (Λ), diffractive order (m), dielectric constant of metal (ε_m) and dielectric (ε_d), and angle of impingement (θ). Because ε_d is different on the front side (air/metal interface) versus the back side (substrate/metal interface), this equation shows why the film free sample has different spectral resonance matching conditions. It is also clear to see that by increasing the front side refractive index (and increasing ε_d), one could tune the two plasmon resonance modes to occur at the same wavelength.

Transmission spectra indicate the spectral location and strength of plasmon resonance. They illustrate the impact of changes in bulk refractive index on the plasmon peaks that occur at both front (ambient/film) and back (substrate) sides of the grating. The main impacts noted will be location of resonance and resonance peak shape (attenuation vs. enhancement, size of enhancement, etc).

The high RI on silver sensor is called matched system because, as seen by the evanescent wave of the plasmon, the interfacial high RI film/air appears to match the substrate. This system has three relevant interfaces: substrate/silver, silver/high RI, and high RI/ambient environment. The sensing capability of the third interface of the matched sensor is probed with refractive index studies, alongside with an unmatched platform, to compare

and contrast the two systems. Figure 2 below shows the layers of both systems. As a note, all transmission spectra are referenced with flat spectra, giving a normalized or enhanced transmission factor.

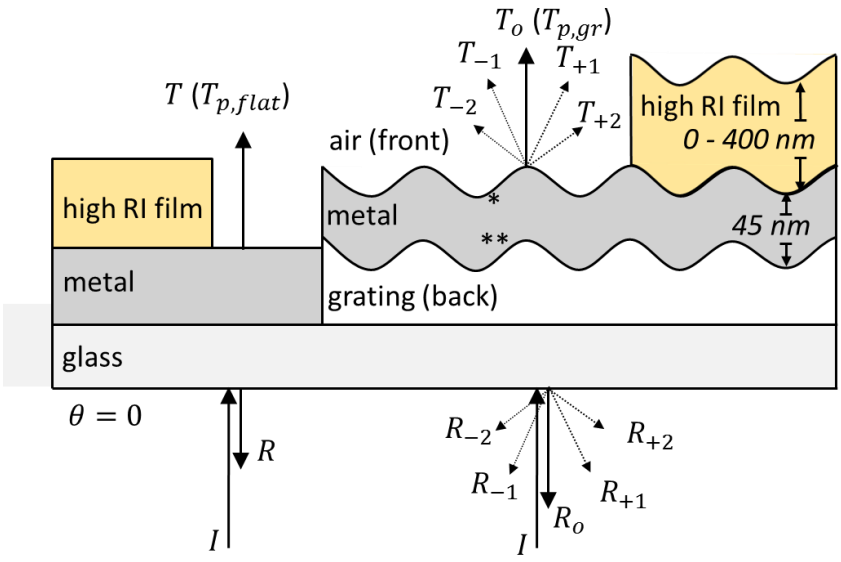

Figure 2.1 Layer geometry of bare silver grating (unmatched) and silver grating with high RI film (matched). Shown are impinging light (*I*), reflected light (*R*), transmitted light (*T*), metal thickness, high refractive index thickness, and diffractive orders. $T_{p,flat}$ is used as the light reference for grating transmission spectra ($T_{p,gr}$) shown in the following figures.

2.4.2 Normal (θ=0°), Unmatched Transmission Spectra Introduction

For optical excitation at normal incidence (θ=0°), the first order diffractive peaks (m = ± 1) produce strong plasmon transmission peaks at both the front (*) and back (**) sides of the metal film, as shown in Figures 2.1 and 2.2. Substituting the grating pitch value as measured for this DVD-R grating (~740 nm) and relative permittivity values for the dielectric (air or polymer substrate) and metal (silver) into the wave vector matching equation, two excitation wavelengths are found: ~755 nm for the front and ~1170 nm for the back side SP peaks.

Experimental transmission spectra (Figure 2.2A) indeed depict two plasmon features at wavelengths consistent to those predicted by Equation 2.1. An enhanced transmission peak is observed at ~760 nm (denoted *) corresponding to the front side plasmon. A dip or attenuation of the transmitted light is observed at longer wavelengths associated with the back side peak (denoted **) at ~1200 nm.

While equation 1 accurately predicts the wavelengths where these resonances appear, it offers little information about the nature of the surface electric field or the resulting spectral enhancement (or attenuation). The experimental results, including the magnitude and location of the peaks, can be predicted with rigorous optical modeling of the grating interface. Figure 2.2B depicts the computed optical transmission spectra for a model of the silver-coated grating using the RCWA model. The predicted response shows a strong similarity to the measured results, with only small differences in the magnitudes of the enhanced and attenuated peaks.

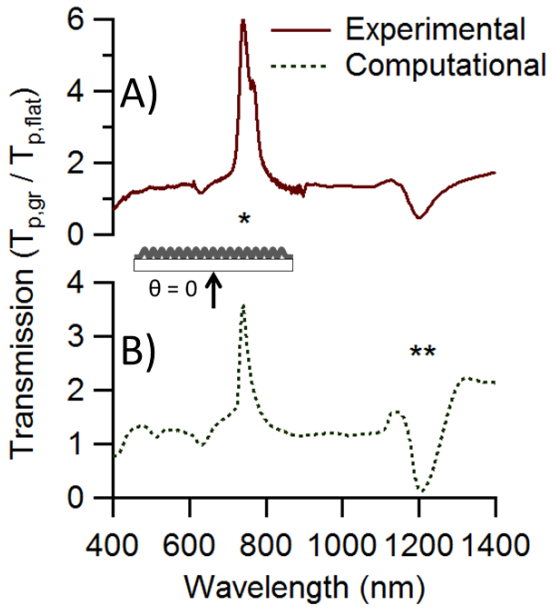

Figure 2.2 Normal impingement visible transmission spectra through silver gratings, referenced with flat silver. Denoted by * and ** are front and back side resonances, respectively. The inset shows normal impingement angle.

2.4.3 Increasing High RI Thickness Transmission Spectra

The presence of two distinct plasmon features as noted in Figure 2.2 is an indication of an asymmetric interface with unmatched plasmon wave vectors on opposing sides of the silver film. In order to create the desired symmetry in this interface, increasingly thicker layers of a high refractive index (RI) tin oxide were coated onto the ambient/front side of the silver grating (geometry shown in Figure 2.1). Reactive DC sputtering of a tin target in the presence of oxygen was optimized to produce SnO2 film. This oxide stoichiometry produces a transparent film with high RI (n). In comparison, the UV curable substrate polymer is also transparent, but with an RI similar to that of optical quality glass (RI values are given in Supporting Information 2.7.2).

Optical transmission measurements for several samples with increasing thickness of tin oxide are shown in Figure 2.3A. While all spectra shown here were collected at normal impingement ($\theta=0°$), dispersion images (angle variable heat maps) were also collected and analyzed (see Supporting Information 2.7.1) At tin oxide thicknesses of 0, 66, and 145 nm, the front side plasmon peak appears at 738, 843 and 1025 nm, respectively. These samples show the expected increase in plasmon wavelength with increasing film thickness (Figure 2.3B), while the back-side resonant location remains unchanged. For the 145 nm tin oxide film, evidence of resonant coupling between the front and back-side modes is beginning to appear as the back side mode transitions from attenuation to enhancement. At a thickness of 244 nm, the front and back-side features are overlapping and a large enhancement peak appears, with a magnitude near 40. Full matching was found to occur with 300-320 nm high RI layer, yielding a transmission enhancement consistently between 80 and 100 times compared to flat silver with an equivalent amount of high RI layer.

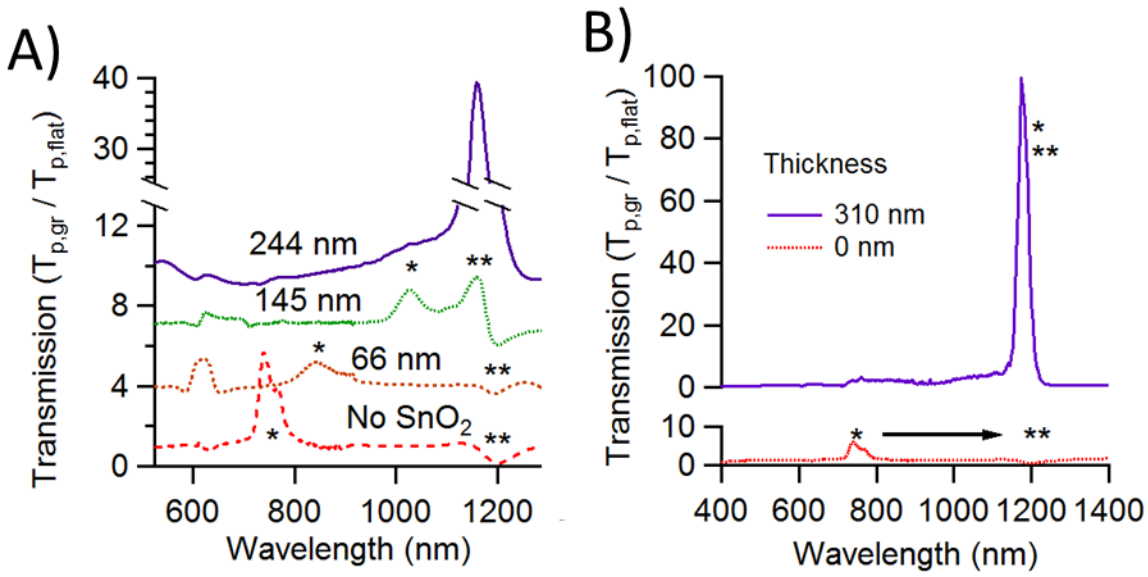

Figure 2.3 Normal impingement visible transmission spectra through silver gratings with increasing tin oxide thickness values (A), referenced with flat silver. Highlighted in B is a comparison of the unamatched system and the matched system on axes of the same scale.

The experimental results were confirmed computationally (Figure 2.4). The RCWA simulation was scanned across SnO_2 thickness values between 0 and 400 nm, shown in Figure 2.4A. Front and back side peak locations were extracted from all viable SnO_2 on Ag grating samples and plotted in Figure 2.4B. It is clear from the figure that the front side progression towards the back side resonance condition is similarly depicted by both experimental and computational methods.

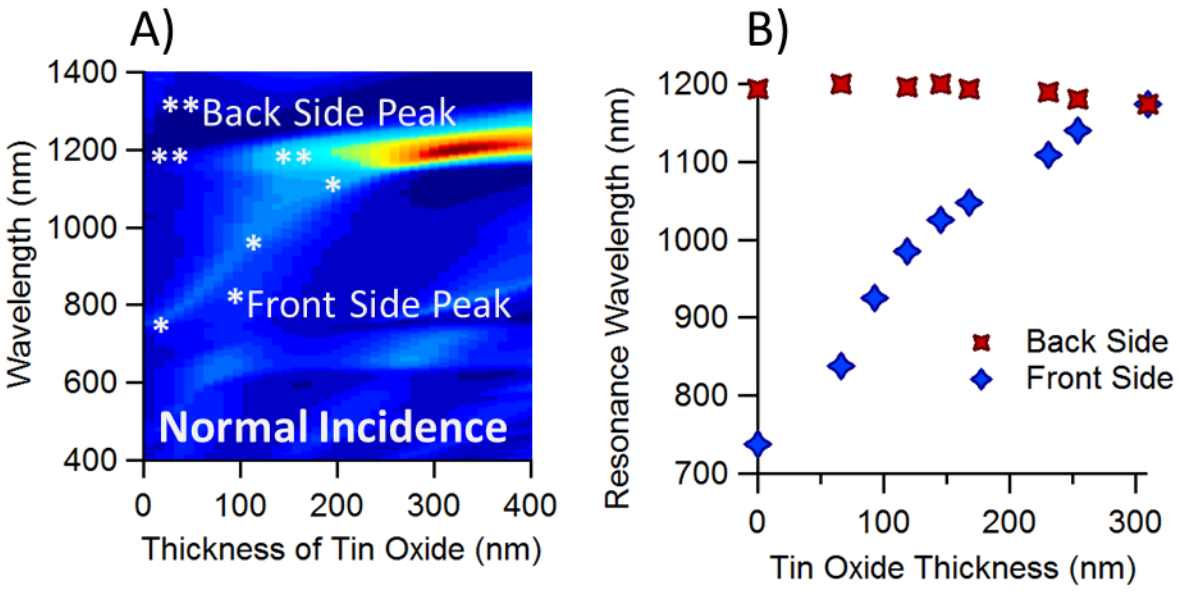

Figure 2.4 Front side and back side peak tracking of normal impingement visible transmission plotted versus increasing tin oxide thickness. Computational results shown on the left and experimental results shown on the right.

2.4.4 Increasing High RI Thickness Computational Analysis

Figure 2.5 below shows computational results for transmission and reflection of TM polarized light through 50 nm of silver with and without tin oxide. Explain the figures more. Connection of these results to previous: explicating the shape of the spectra.

The unmatched system shows decoupled modes where the front side peak allows for reflected light to come through as transmission (Figure 2.5A, I). The back side peak acts as a strong reflector (Figure 2.5A, II). When sufficient high refractive index is deposited (300 nm), the front side overlaps with the back side, allowing for light previously reflected and absorbed to be transmitted through the front side resonance (Figure 2.5B, III). Since this front side resonance allows for resonant energy transfer from the back side plasmon mode to transmit, there is probably a large localized electric field associated with it.

Despite knowing physical locations of SPR in the grating layers and the transmission and reflection enhancements values (described in previous paragraph), explaining these shapes is somewhat speculative. It is proposed here that the front side resonance of the unmatched grating efficiently transmits reflected light at 740 nm but inefficiently transfers the light from the back side of the silver grating due to losses in the metal. At the back side resonance, it is uncertain why the reflection maintains at 1, but it is almost certain that the transmission diminishes due to the resonance mode localizing the electromagnetic wave at 1200 nm on the back side, which is then absorbed in the metal. Upon matching the front and back side resonance modes, light efficiently transfers across the thin metal film between the two modes at 1200 nm, indicated by reflection diminishing to zero and transmission increasing over an order of magnitude.

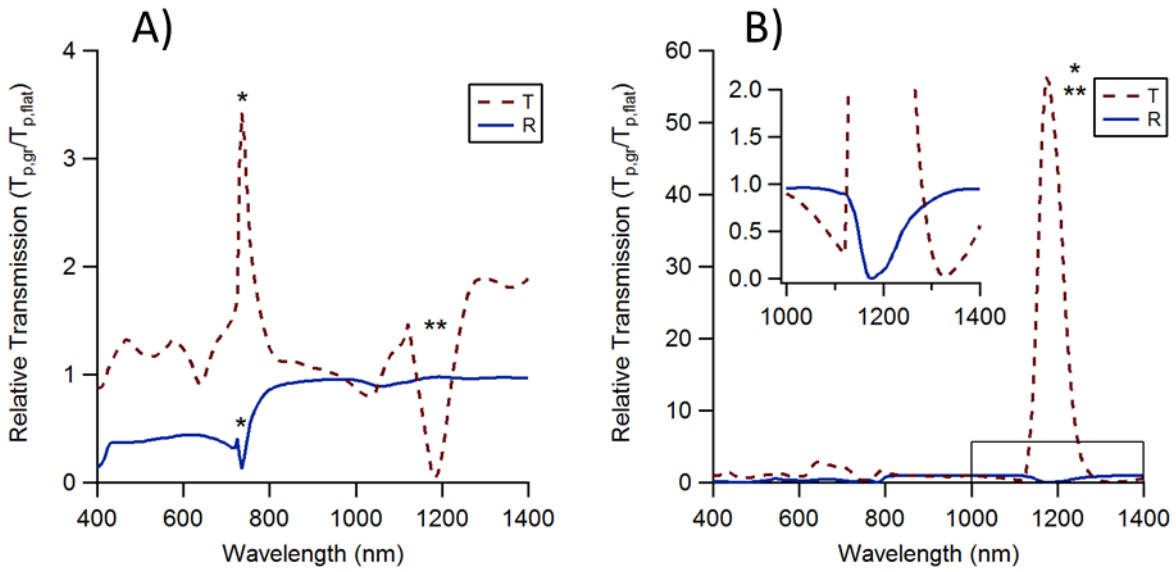

Figure 2.5 Computational spectra of transmitted and reflected light of film free (unmatched) silver gratings and high RI film (matched) gratings. Denoted by * is the front side peak, where relative transmission increases beyond 1, while reflection diminishes. Denoted by ** is the back side resonance where the transmission diminishes to 0 but reflection maintains at 1. Denoted by */** in B is the overlap of front and back side resonance modes, showing a dramatic increase in transmission beyond 1, and a decrease in reflection to 0.

2.4.5 Probing Matched and Unmatched System with RI Sensing

To analyze the analytical capabilities of the matched versus unmatched systems, refractive index sensing was performed with mixtures of glycerol and water. Computational and experimental data were collected at refractive indexes of 1.33, 1.4 and 1.475 using a 1:0, 1:1, and 0:1 ratio of DIW (n=1.33) and glycerol (n=1.475).

First, presented in Figure 2.6A below are experimental results for RI studies for the unmatched system (silver on grating, no SnO2). As expected, with increasing front side RI, the front side resonance mode shifts from 741 nm in air, to 987 nm in DIW, 1045 nm in the 1:1 mixture, and 1097 in glycerol. The calculated sensitivity for the unmatched system is 752 nm/RI empirically and 824 nm/RI computationally. Because the water and glycerol RI are close to that of the substrate (n=1.5), the back side resonance modes show increasing intensity with increasing RI.

Shown in Figure 2.6B are experimental results for the matched system (silver on grating with 310 nm SnO2). Observed in these spectra is a diminished wavelength shift sensitivity and increased intensity sensitivity with a change in front side RI. As front side RI is increased from 1.33 with DIW to 1.475 in glycerol, the intensity can be seen to decrease from 20% to 12%. The calculated sensitivity for this regime is -68 AU/RI empirically and -35 AU/RI computationally.

Figure 2.6C/D show the wavelength and transmission intensity for both matched and unmatched samples. It can be seen that the nature of the RI sensor changes from wavelength tracking for unmatched conditions to intensity tracking for matched conditions.

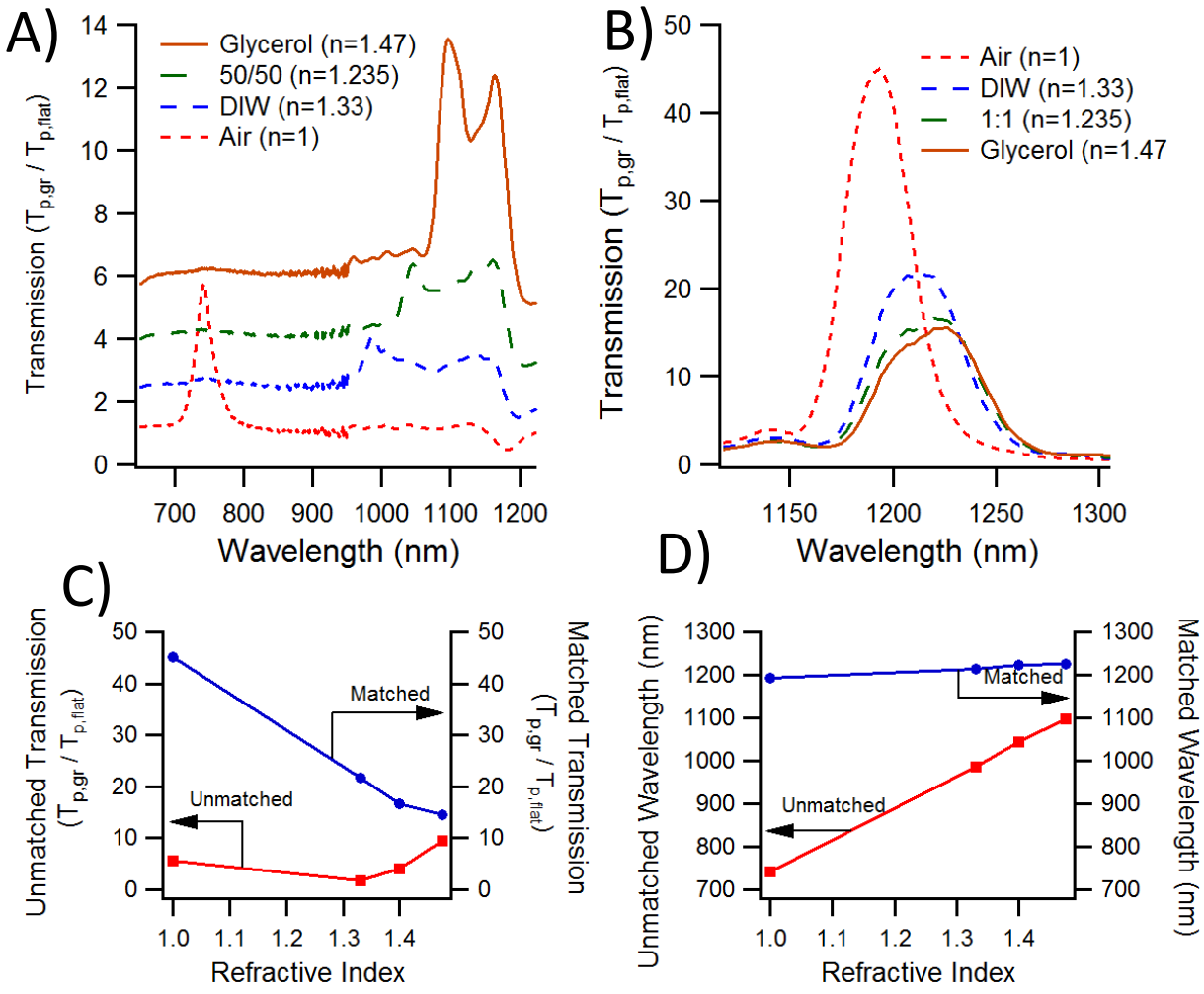

Figure 2.6 Refractive index sensing of matched and unmatched grating systems. Unmatched sensor (A) shows wavelength tracking of front side peak location with increase in RI. Matched sensor (B) shows change in intensity and slight change in wavelength

2.5 Conclusion

The unmatched system shows the expected response and sensitivity of classic GC-SPR sensors, allowing the change in wavelength to be tracked for binding or bulk RI sensitivity. By altering the front side optical condition and resonance mode to match the back side, the two modes couple and enhance. Because the high refractive index layer extends 300 nm into the largest portion of the evanescent wave, the front side RI increase as seen by the

evanescent wave will not substantially change the resonant wavelength with amount bound or bulk RI. The enhancement decrease that is observed is the matching condition becoming unmatched as the effective front side RI is increased past that of the back side.

While it is important to realize that the unmatching due to a change in front side RI allows this system to be used as a unique way to analyze amount bound and changes in bulk RI, there is a deeper implication to these results. The shifts in spectral intensity of the coupled resonance modes as they are pushed off resonance indicate an altering of the local media within the evanescent wave. If this is the case, the drastic increase in transmission intensity from the unmatched to matched system would allow for possibility of coupling of spectroscopic transitions to these strong resonance modes.

2.6 Acknowledgements

This work was supported by the National Science Foundation (Grant CHE 1213582).

2.7 Supporting Information

2.7.1 Additional Results: Dispersion Images and Simulations

Dispersion images are compilations of spectra collected at varied angles of impingement. Dispersion images in this study contain spectra at angles ranging between -60° and +60° with respect to normal incidence. These images were collected using the motorized rotation stage in conjunction with a homebuilt control program (LabView), as described previously[38] and plotted as 3D heat images in Matlab. Select images of interest are shown in Figure 2.7. The dispersion images show various features, mostly consisting of lines that

represent dispersing (angle- and wavelength-dependent) plasmon modes associated with specific diffracted orders.

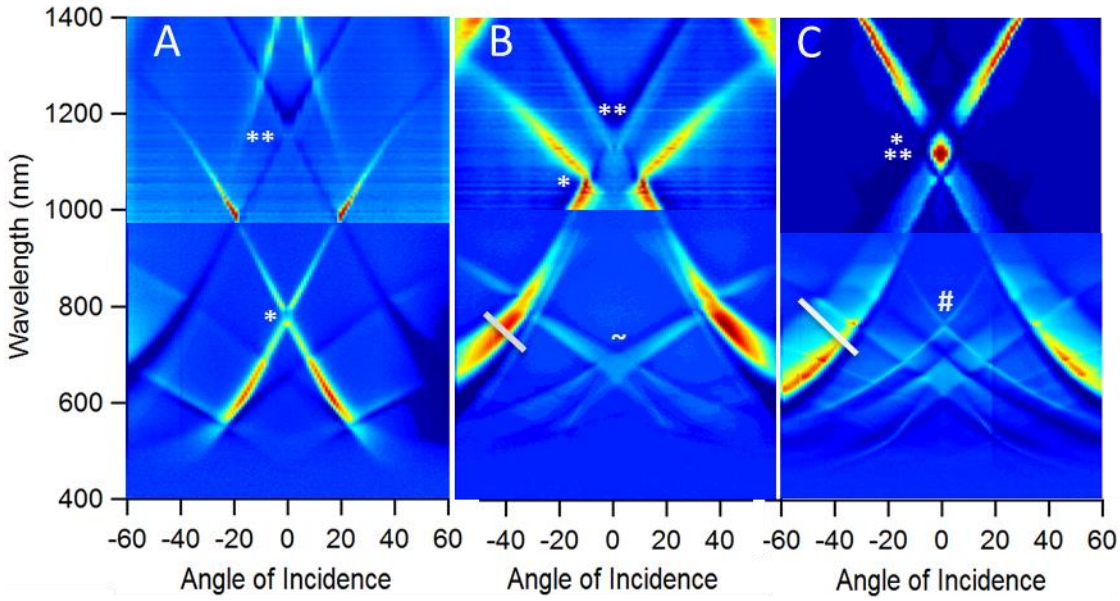

Figure 2.7 Dispersion images showing relative transmission ($T_{p,gr}/T_{p,flat}$) as a function of wavelength and incident angle for (A) 0 nm, (B) 128 nm, and (C) 323 nm tin oxide films. The images have been contrast adjusted to best illustrate the various transmission features. Various features noted in figure are described in the text.

Figure 2.7A shows the dispersion image for the bare silver grating. The first order diffracted modes for the front side (*) of the grating appear as enhanced optical transmission, with lines of enhancement that vary with angle and cross at ~755 nm. The SP modes associated with first order diffraction from the back side (**) of the grating appear as dark lines (or attenuation) that cross at ~1200 nm. Plotting the data from a vertical line through 0° would produce the transmission spectra as shown in Figure 2.2 for the bare grating.

Figure 2.7B depicts a dispersion image for the grating after coating with a 128 nm tin oxide film. There is a shift in the front side features (*) to longer wavelengths, while the back side features (**) have not moved. The high intensity bands at angles and wavelengths around +/- 40° and 700 nm, respectively, are substantially enhanced and appear to be from

overlapping front and back side features that are index matched (denoted —). At longer wavelengths and smaller angles, the front (*) and back (**) side features do not yet appear matched at this layer thickness, although there is an apparent quenching of the front side peaks near 0°. Another feature that appears at lower wavelengths is a set of crossing lines centered at ~650 nm (denoted ~), which are attributed to weaker plasmon modes associated with second order diffraction from the front side of the grating.

The third dispersion image (Figure 2.7C), a silver grating replica with a 323 nm tin oxide film, shows a very large enhancement at normal incidence. This large peak at ~1200 nm (denoted ⁂) demonstrates the desired index matching at normal incidence. Enhancements are also seen at longer wavelengths (> 1200 nm) and larger angles, where the peaks split into +/- 1 diffracted modes. At larger angles and lower wavelengths, there is continued evidence for matching of the front and back-side plasmon peaks (denoted —) as was observed in Figure 2.7B. However, the front side peaks have now passed the back-side and produce an increased span of enhancement with decreased peak intensity (as compared to Figure 2.7B). Nevertheless, the front and back side modes still appear coupled as indicated by continued transmission enhancement. At lower wavelengths, there is also evidence for the appearance of guided modes as very thin crossing lines (denoted by #), as is expected with this thick tin oxide layer now acting as a waveguide.

The experimental transmission results (Figure 2.3) and dispersion images (Figure 2.7) confirm that that wave vector matching can be achieved by coating with a tin oxide film. Where the matching occurs, and the optimum film thickness, both vary as a function of wavelength and angle due to the differences in refractive index of materials on the front and back of the grating. This behavior, and prediction of the optimum film thicknesses required

for index matching, can be deduced via optical modeling. In Figure 2.8, we show the grating profile used for optical modeling (Figure 2.8A) and predicted transmission at two different incident angles (Figure 2.8B and C) as a function of wavelength and increasing tin oxide thickness. Lines are drawn through the front side (*) and back side (**) peaks as a guide.

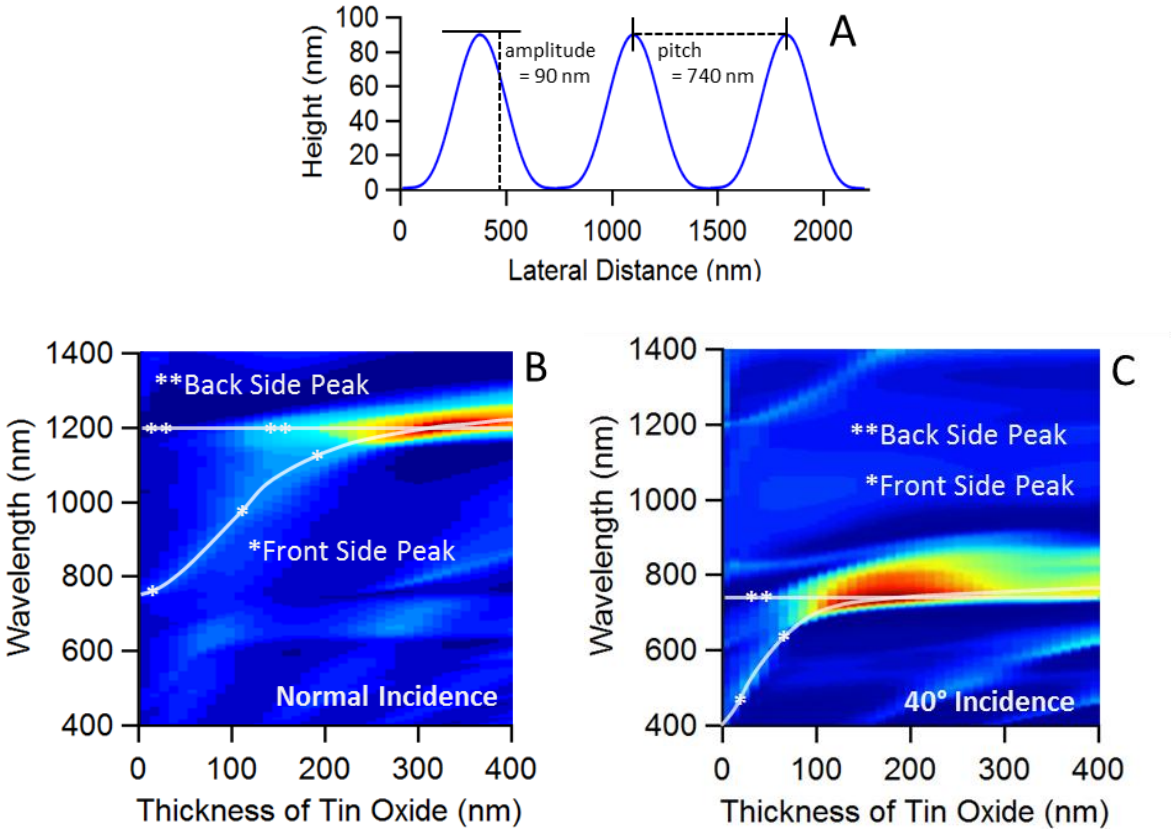

Figure 2.8. (A) Schematic of grating surface profile used for computational models. Predicted transmission intensity as a function of wavelength and tin oxide thickness at incident angles of (B) 0° and (C) 40°.

At, $\theta = 0°$ (Figure 2.8B) the front side peak begins as a small enhancement at 738 nm with no tin oxide layer. With increasing tin oxide thickness, the front side peak moves to longer wavelengths until it approaches the backside peak. As the peaks overlap, the transmission intensity increases and then reaches a maximum transmission intensity for a ~300 nm tin oxide layer. Over this range of thicknesses, the back-side peak is mostly

unchanged, but merges with the front side peak as they begin to overlap. Similar results predicted for the response at an incident angle of $\theta = 40°$ indeed shows slightly different behavior (Figure 2.8B). In this result, we see the initial plasmon peak for the front side at ~500 nm and the back-side at ~800 nm. The front side peak also moves towards longer wavelengths with increasing tin oxide film thickness, while the back-side does not move. In this case, the overlap appears at much thinner film thicknesses, as expected, with an optimum at only ~100 nm of tin oxide.

2.7.2 Thin Film Analysis: Ellipsometry

Spectroscopic ellipsometry measures the change in polarization of reflected light. This change is represented by a change in amplitude (phi) and phase (delta) of p- and s-polarized light. These two parameters depend on the optical properties and thickness of the material. With ideal systems, ellipsometry data can be used to find the optical properties or thickness, if the other is known. However, physical parameters such as surface roughness, gradients in layers, and other material properties effect the spectra collected. Modeling of these physical parameters, optical properties and layer thickness enables one to solve for many unknowns with collected ellipsometry spectra.

Modern ellipsometer units (like Alpha-SE from J. A. Woollam Co., used in this lab) often come equipped with powerful software (CompleteEASE in this case) that allow for such modeling. CompleteEASE was used in this experiment to obtain the thickness of the SnO2 layer deposited on a clean glass slide concurrently with the silver SPR slide (as described in the methods above). To begin, a two layer structure is chosen to represent our system, as shown in figure 2.9.

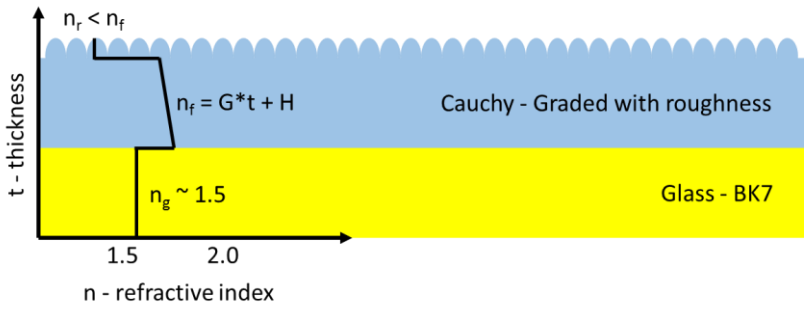

Figure 2.9 Refractive index profile as solved for by CompleteEASE software when considering a surface roughness layer and graded superstrate refractive index.

The substrate was known, so its optical properties were held constant according to the values provided by the software. Tin oxide is a transparent glass and can be modeled as a Cauchy material with the dispersion relation given in equation S1 below, where A, B and C are constants that can be solved for.

$$n(\lambda) = A + \frac{B}{\lambda^2} + \frac{C}{\lambda^4}$$

Having a homogenous layer for the tin oxide poorly fit the collected ellipsometry spectra. By allowing (1) the Cauchy material to vary linearly from bottom to top and (2) a 50% void roughness layer to exist within the model, the error of the fit was minimized. This makes sense as the density and crystal structure may vary throughout the layer and it is expected that the layer will have surface roughness. The roughness layer is 50% void and optimized in thickness. Example optical constants varying from top to bottom are shown in Figure 2.10.

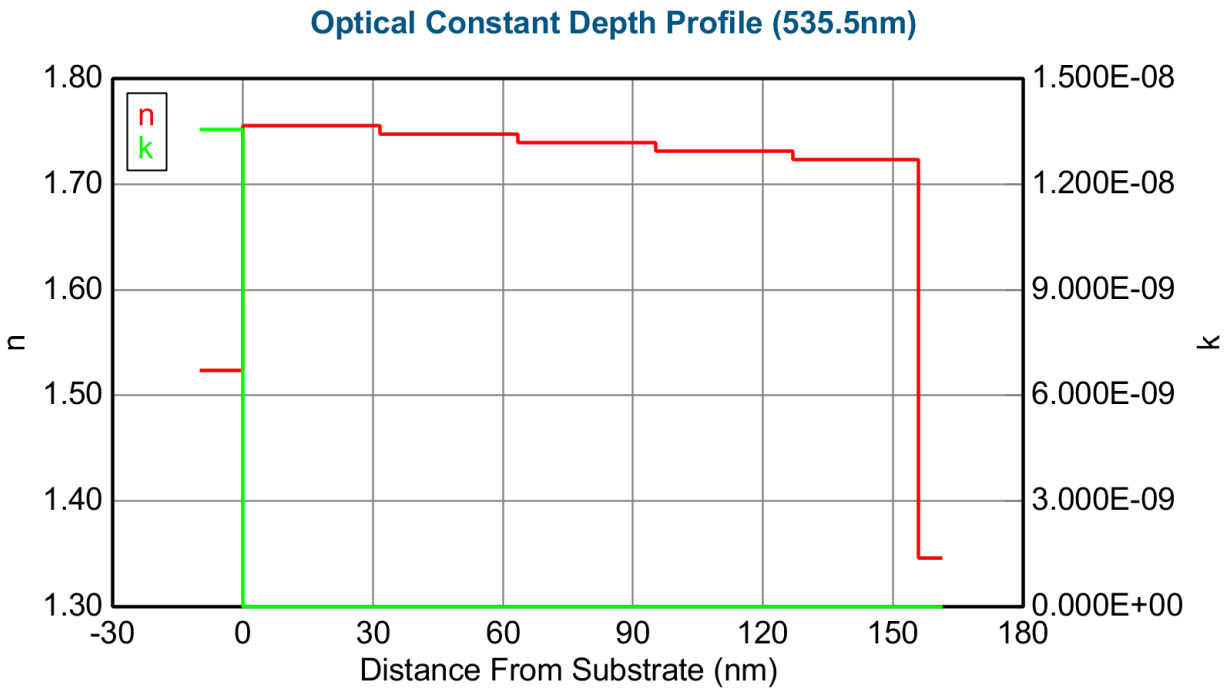

Figure 2.10 Example refractive index profile showing glass RI at the far left, 5 steps for graded layer, and roughness layer at the far right.

The varying is seen as a 5 step changes, as the software models this linear variance as several discrete slabs (the number is chosen by user). The average change from bottom to top was between -1% and -5%.

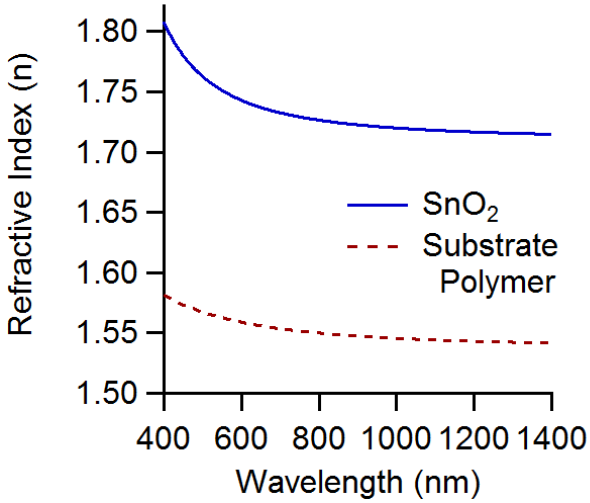

Figure 2.11 Refractive index values for high RI film (SnO_2) and substrate polymer (NOA61) as a function of wavelength in the visible and NIR regime.

2.7.3 RCWA Modeling

The rigorously-coupled wave analysis method solves for optical responses of multilayer interfaces such as the one used in this study. The grating is broken into slabs vertically and a Fourier expansion is performed on the electric field within each slab. This system of equations is solved to obtain eigenvalues and eigenvectors. The boundary conditions of the slabs are then matched to obtain the overall grating diffraction efficiency.

To make the problem tractable, a finite number of orders of the Fourier transform are retained. Accuracy can be obtained by plotting diffraction efficiency versus number of retained orders until convergence. Authors Lalanne and Morris (1996) proposed a different formulation for the Eigen value problem cause convergence with fewer orders. This formulation was used in the RCWA protocol developed in MatLab in this lab.

Parameters of the simulation and their typical values were maximum slab size (5 nm), starting wavelength (400 nm), final wavelength (1400 nm), wavelength step increment (5 nm), wavelength dependent optical properties (see methods in paper), amplitude of grating (90 nm), thickness of silver (45 nm), thickness of SnO2 (0-400 nm) and grating shape (see results).

The grating shape was based off a power sine representation of the DVD profile having a grating pitch of 740 nm and amplitude of 90 nm, as measured by atomic force microscopy for these samples. The silver layer was 45 nm thick and published wavelength dependent optical constants were used[148]. The tin oxide layer thickness was varied to match the measured values and Cauchy optical constants derived from ellipsometry were used for

the refractive index. The manufacturer supplied a Cauchy formula for their UV curable polymer and this was used as the refractive index of the substrate.

2.8 References

(1) Wood, R. W. *Proc. Phys. Soc. London* **1902**, *18* (1), 269.
(2) Wood, R. W. *Philos. Mag. Ser. 6* **1912**, *23* (134), 310–317.
(3) Rayleigh, Lord. *Proc. R. Soc. London. Ser. A, Contain. Pap. a Math. Phys. Character* **1907**, *79* (532), 399–416.
(4) Hessel, A.; Oliner, A. A. *Appl. Opt.* **1965**, *4* (10), 1275.
(5) Ritchie, R. H. *Phys. Rev.* **1957**, *106* (5), 874–881.
(6) Powell, C. J.; Swan, J. B. *Phys. Rev.* **1960**, *118* (3), 640–643.
(7) Bohm, D.; Pines, D. *Phys. Rev.* **1951**, *82* (5), 625–634.
(8) Pines, D.; Bohm, D. *Phys. Rev.* **1952**, *85* (2), 338–353.
(9) Bohm, D.; Pines, D. *Phys. Rev.* **1953**, *92* (3), 609–625.
(10) Burstein, E. *J. Vac. Sci. Technol.* **1974**, *11* (6), 1004.
(11) Kretschmann, E.; Raether, H. *Zeitschrift Fuer Naturforschung, Tl. A* **1968**, *23* (November 1968), 2135.
(12) Kretschmann, E. *Zeitschrift für Phys.* **1971**, *241* (4), 313–324.
(13) Otto, A. *Zeitschrift für Phys.* **1968**, *216* (4), 398–410.
(14) Liedberg, B.; Nylander, C.; Lunström, I. *Sensors and Actuators* **1983**, *4*, 299–304.
(15) Pockrand, I.; Swalen, J. D.; Gordon, J. G.; Philpott, M. R. *Surf. Sci.* **1978**, *74* (1), 237–244.
(16) Peterlinz, K. A.; Georgiadis, R. *Opt. Commun.* **1996**, *130* (4-6), 260–266.
(17) Liedberg, B.; Lundström, I.; Stenberg, E. *Sensors Actuators B Chem.* **1993**, *11* (1-3), 63–72.
(18) Striebel, C.; Brecht, A.; Gauglitz, G. *Biosens. Bioelectron.* **1994**, *9* (2), 139–146.
(19) Cullen, D. C.; Brown, R. G. W.; Lowe, C. R.; Culle, D. C.; Brown, R. G. W.; Lowe, C. R. *Biosensors* **1987**, *3* (4), 211–225.
(20) Jory, M. J.; Bradberry, G. W.; Cann, P. S.; Sambles, J. R. *Meas. Sci. Technol.* **1995**, *6* (8), 1193.
(21) Lawrence, C. R.; Geddes, N. J.; Furlong, D. N.; Sambles, J. R. *Biosens. Bioelectron.* **1996**, *11* (4), 389–400.
(22) Moskovits, M. *Rev. Mod. Phys.* **1985**, *57* (3), 783–826.
(23) Willets, K. A.; Van Duyne, R. P. *Phys. Chem.* **2007**, *58*, 267–297.
(24) Haynes, C. L.; Van Duyne, R. P. *J. Phys. Chem. B* **2001**, *105* (24), 5599–5611.
(25) Homola, J.; Yee, S. S.; Gauglitz, G. *Sens. Actuators, B* **1999**, *54* (1–2), 3–15.
(26) Meneghello, A.; Antognoli, A.; Sonato, A.; Zacco, G.; Ruffato, G.; Cretaio, E.; Romanato, F. *Anal. Chem.* **2014**, *86* (23), 11773–11781.
(27) Yu, F.; Tian, S.; Yao, D.; Knoll, W. *Anal. Chem.* **2004**, *76* (13), 3530–3535.
(28) Silvestri, D.; Sonato, A.; Ruffato, G.; Meneghello, A.; Antognoli, A.; Cretaio, E.; Dettin, M.; Zamuner, A.; Casarin, E.; Zacco, G.; Romanato, F.; Morpurgo, M. *Anal. Methods* **2015**, *7* (10), 4173–4180.

(29) Singh, B. K.; Hillier, A. C. *Anal. Chem.* **2007**, *79* (14), 5124–5132.
(30) Wang, Y.; Brunsen, A.; Jonas, U.; Dostalek, J.; Knoll, W. *Anal. Chem.* **2009**, *81* (23), 9652.
(31) Zhu, H.; Snyder, M. *Curr. Opin. Chem. Biol.* **2003**, *7* (1), 55–63.
(32) Crespo-Biel, O.; Dordi, B.; Reinhoudt, D. N.; Huskens, J. *J. Am. Chem. Soc.* **2005**, *127* (20), 7594–7600.
(33) Jorgenson, R. C.; Yee, S. S. *Sens. Actuators, A* **1994**, *43* (1–3), 44–48.
(34) Mao, Y.; Bao, Y.; Wang, W.; Li, Z.; Li, F.; Niu, L. *Talanta* **2011**, *85* (4), 2106–2112.
(35) Pei, R. J.; Cui, X. Q.; Yang, X. R.; Wang, E. K. *Biomacromolecules* **2001**, *2* (2), 463–468.
(36) Petefish, J. W.; Hillier, A. C. *Anal. Chem.* **2014**, *86* (5), 2610–2617.
(37) Singh, B. K.; Hillier, A. C. *Anal. Chem.* **2006**, *78* (20), 7335–7340.
(38) Yeh, W.-H.; Hillier, A. C. *Anal. Chem.* **2013**, *85* (8), 4080–4086.
(39) Yeh, W.-H.; Petefish, J. W.; Hillier, A. C. *Anal. Chem.* **2011**, *83* (15), 6047–6053.
(40) Yeh, W.-H.; Petefish, J. W.; Hillier, A. C. *Anal. Chem.* **2012**, *84* (2), 1139–1145.
(41) Homola, J. *Anal. Bioanal. Chem.* **2003**, *377* (3), 528–539.
(42) Couture, M.; Zhao, S. S.; Masson, J.-F. *Phys. Chem. Chem. Phys.* **2013**, *15* (27), 11190–11216.
(43) Homola, J. J. *Chem. Rev.* **2008**, *108* (2), 462–493.
(44) Cooper, M. A. *Nature Reviews Drug Discovery*. 2002, pp 515–528.
(45) Myszka, D. G. *J. Mol. Recognit.* **1999**, *12* (5), 279–284.
(46) Huang, Y.-F.; Zhang, M.; Zhao, L.-B.; Feng, J.-M.; Wu, D.-Y.; Ren, B.; Tian, Z.-Q. *Angew. Chemie Int. Ed.* **2014**, *53* (9), 2353–2357.
(47) Lal, S.; Grady, N. K.; Kundu, J.; Levin, C. S.; Lassiter, J. B.; Halas, N. J. *Chem. Soc. Rev.* **2008**, *37* (5), 898–911.
(48) Nie, S.; Emory, S. R. *Science (80-.).* **1997**, *275* (5303), 1102–1106.
(49) Campion, A.; Kambhampati, P.; Campion, A.; Kambhampati, P. *Chem. Soc. Rev.* **1998**, *27* (4), 241–250.
(50) Zhou, F.; Liu, Y.; Cai, W. *Opt. Lett.* **2014**, *39* (5), 1302–1305.
(51) Miyake, H.; Ye, S.; Osawa, M. *Electrochem. Commun.* **2002**, *4* (12), 973–977.
(52) Le, F.; Brandl, D. W.; Urzhumov, Y. A.; Wang, H.; Kundu, J.; Halas, N. J.; Aizpurua, J.; Nordlander, P. *ACS Nano* **2008**, *2* (4), 707–718.
(53) Smolyaninov, I. I.; Hung, Y. J.; Davis, C. C. *Conf. Quantum Electron. Laser Sci. - Tech. Dig. Ser.* **2007**, *14* (22), 10825–10830.
(54) Huang, C.-J.; Dostalek, J.; Sessitsch, A.; Knoll, W. *Anal. Chem.* **2011**, *83* (3), 674–677.
(55) Chun Jen, H.; Jakub, D.; Wolfgang, K. *J. Vac. Sci. Technol., B Microelectron. Nanom. Struct.* **2010**, *28*, 66.
(56) Ekgasit, S.; Thammacharoen, C.; Yu, F.; Knoll, W. *Anal. Chem.* **2004**, *76* (8), 2210–2219.
(57) Kasry, A.; Knoll, W. *Appl. Phys. Lett.* **2006**, *89* (10), 101103–101106.
(58) Lakowicz, J. R. *Anal. Biochem.* **2004**, *324* (2), 153–169.
(59) Bauch, M.; Toma, K.; Toma, M.; Zhang, Q.; Dostalek, J. *Plasmonics* **2014**, *9* (4), 781–799.
(60) Lakowicz, J. R.; Ray, K.; Chowdhury, M.; Szmacinski, H.; Fu, Y.; Zhang, J.; Nowaczyk, K. *Analyst* **2008**, *133* (10), 1308.

(61) Ekgasit, S.; Yu, F.; Knoll, W.; Biosensor, S. *Langmuir* **2005**, *21* (9), 4077–4082.
(62) Hecht, B.; Sick, B.; Wild, U. P.; Deckert, V.; Zenobi, R.; Martin, O. J. F.; Pohl, D. W. *J. Chem. Phys.* **2000**, *112* (18), 7761–7774.
(63) Qiu, D.; Zhang, D.; Chen, Y.; Zhu, L.; Han, L.; Wang, P.; Ming, H.; Badugu, R.; Lakowicz, J. R. *Opt. Lett.* **2014**, *39* (15), 4341–4344.
(64) Beck, F. J.; Polman, A.; Catchpole, K. R. *J. Appl. Phys.* **2009**, *105* (11), 114310–114317.
(65) Kamat, P. V. *J. Phys. Chem. C* **2007**, *111* (7), 2834–2860.
(66) Linic, S.; Christopher, P.; Ingram, D. B. *Nat Mater* **2011**, *10* (12), 911–921.
(67) Pillai, S.; Catchpole, K. R.; Trupke, T.; Green, M. A. *J. Appl. Phys.* **2007**, *101* (9), 93105–93108.
(68) Yoon, W.-J.; Jung, K.-Y.; Liu, J.; Duraisamy, T.; Revur, R.; Teixeira, F. L.; Sengupta, S.; Berger, P. R. *Sol. Energy Mater. Sol. Cells* **2010**, *94* (2), 128–132.
(69) West, P. R.; Ishii, S.; Naik, G. V.; Emani, N. K.; Shalaev, V. M.; Boltasseva, A. *Laser Photonics Rev.* **2010**, *4* (6), 795–808.
(70) Kretschmann, E. *Opt. Commun.* **1972**, *5* (5), 331–336.
(71) Ritchie, R. H. *Phys. status solidi* **1970**, *39* (1), 297–308.
(72) Nagpal, P.; Lindquist, N. C.; Oh, S.-H.; Norris, D. J. *Science (80-.).* **2009**, *325* (5940), 594–597.
(73) Gryczynski, I.; Malicka, J.; Jiang, W.; Fischer, H.; Chan, W. C. W.; Gryczynski, Z.; Grudzinski, W.; Lakowicz, J. R. *J. Phys. Chem. B* **2005**, *109* (1), 1088–1093.
(74) Abbas, A.; Linman, M.; Cheng, Q. *Biosens. Bioelectron.* **2011**, *26* (5), 1815–1824.
(75) Kaplan, B.; Guner, H.; Senlik, O.; Gurel, K.; Bayindir, M.; Dana, A. *Plasmonics* **2009**, *4* (3), 237–243.
(76) Giannattasio, A.; Barnes, W. *Opt. Express* **2005**, *13* (2), 428–434.
(77) Magnusson, R.; Svavarsson, H. G.; Yoon, J.; Shokooh-Saremi, M.; Song, S. H. *Appl. Phys. Lett.* **2013**, *100* (9), 091106.
(78) Chang, S.-H.; Gray, S.; Schatz, G. *Opt. Express* **2005**, *13* (8), 3150–3165.
(79) Halpern, A. R.; Corn, R. M. *ACS Nano* **2013**, *7* (2), 1755–1762.
(80) Lindquist, N. C.; Nagpal, P.; Lesuffleur, A.; Norris, D. J.; Oh, S.-H. *Nano Lett.* **2010**, *10* (4), 1369–1373.
(81) Chung, A. J.; Huh, Y. S.; Erickson, D. *Nanoscale* **2011**, *3* (7), 2903–2908.
(82) Wang, S.; Pile, D. F. P.; Sun, C.; Zhang, X. *Nano Lett.* **2007**, *7* (4), 1076–1080.
(83) Franzen, S. *J. Phys. Chem. C* **2008**, *112* (15), 6027–6032.
(84) Chiu, N.-F.; Lin, C.; Lee, J.-H.; Kuan, C.; Wu, K.; Lee, C.; Yu, C.; Nien, S.-Y.; Lee, J.-H.; Kuan, C.; Wu, K.; Lee, C.; Lin, C.; Nan-Fu, C.; Chii-Wann, L.; Jiun-Haw, L.; Chieh-Hsiung, K.; Kuang-Chong, W.; Chih-Kung, L. *Appl. Phys. Lett.* **2007**, *91* (8), 83114.
(85) Petefish, J. **2014**.
(86) Chegel, V.; Whitcombe, M. J.; Turner, N. W.; Piletsky, S. A. *Biosens. Bioelectron.* **2009**, *24* (5), 1270–1275.
(87) Moharam, M. G.; Gaylord, T. K. *J. Opt. Soc. Am. A* **1986**, *3* (11), 1780–1787.
(88) Moharam, M. G.; Grann, E.; Pommet, D.; Gaylord, T. K. *J. Opt. Soc. Am. A* **1995**, *12* (5), 1068–1076.
(89) Moharam, M. G.; Pommet, D.; Grann, E.; Gaylord, T. K. *J. Opt. Soc. Am. A* **1995**, *12* (5), 1077–1086.

(90) Knoll, W. *Annu. Rev. Phys. Chem.* **1998**, *49* (1), 569–638.
(91) MAIER, S. A. *Plasmonics: Fundamentals and Applications*; Springer: 233 Spring Street, New York, NY 10013, USA, 2007; Vol. 1.
(92) Boersch, H.; Geiger, J.; Imbusch, A.; Niedrig, N. *Phys. Lett.* **1966**, *22* (2), 146–147.
(93) Sarid, D. *Phys. Rev. Lett.* **1981**, *47* (26), 1927–1930.
(94) Stegeman, G. I.; Burke, J. J.; Hall, D. G. *Opt. Lett.* **1983**, *8* (7), 383.
(95) Burke, J. J.; Stegeman, G. I.; Tamir, T. *Phys. Rev. B* **1986**, *33* (8), 5186–5201.
(96) Wang, Y.; Knoll, W.; Dostalek, J. *Anal. Chem.* **2012**, *84* (19), 8345–8350.
(97) Dostálek, J.; Roskamp, R. F.; Knoll, W. *Sensors Actuators B Chem.* **2009**, *139* (1), 9–12.
(98) Nenninger, G. G.; Tobiška, P.; Homola, J.; Yee, S. S. *Sens. Actuators, B* **2001**, *74* (1–3), 145–151.
(99) Dostálek, J.; Kasry, A.; Knoll, W. *Plasmonics* **2007**, *2* (3), 97–106.
(100) Joo, Y. H.; Song, S. H.; Magnusson, R. *Opt. Express* **2009**, *17* (13), 10606.
(101) Huang, C. J.; Dostalek, J.; Knoll, W. *Biosens. Bioelectron.* **2010**, *26* (4), 1425–1431.
(102) Ishikawa-Ankerhold, H. C.; Ankerhold, R.; Drummen, G. *Molecules*. 2012, pp 4047–4132.
(103) Noomnarm, U.; Clegg, R. *Off. J. Int. Soc. Photosynth. Res.* **2009**, *101* (2), 181–194.
(104) *Curr. Biol.* **1994**, *4* (5), 443.
(105) Yang, T.-T.; Kain, S. R.; Kitts, P.; Kondepudi, A.; Yang, M. M.; Youvan, D. C. *Gene* **1996**, *173* (1), 19–23.
(106) Chen, W.; Long, K. D.; Yu, H.; Tan, Y.; Choi, J. S.; Harley, B. a; Cunningham, B. T. *Analyst* **2014**, *139* (22), 5954–5963.
(107) Basché, T. *J. Lumin.* **1998**, *76-77*, 263–269.
(108) Patterson, G. H. *Semin. Cell Dev. Biol.* **2009**, *20* (8), 886–893.
(109) Geddes, C. D.; Lakowicz, J. R. *J. Fluoresc.* **2002**, *12* (2), 121–129.
(110) Szmacinski, H.; Lakowicz, J. R. *Anal. Chem.* **2008**, *80* (16), 6260–6266.
(111) Liebermann, T.; Knoll, W. *Colloids Surf., A* **2000**, *171* (1–3), 115–130.
(112) Kim, K.; Kim, D. J.; Kim, D. *Quantum Dots, Part. Nanoclusters Vi* **2009**, *7224*, SPIE.
(113) Hao, Y.; Wang, H.; Zhang, Z.; Zhang, X. L.; Chen, Q.; Sun, H. *J. Phys. Chem. C* **2013**, *117* (50), 26734–26739.
(114) Neumann, T.; Johansson, M.-L.; Kambhampati, D.; Knoll, W. *Adv. Funct. Mater.* **2002**, *12* (9), 575–586.
(115) Lakowicz, J. R.; Shen, Y.; D'Auria, S.; Malicka, J.; Fang, J.; Gryczynski, Z.; Gryczynski, I. *Anal. Biochem.* **2002**, *301* (2), 261–277.
(116) Gryczynski, I.; Malicka, J.; Gryczynski, Z.; Lakowicz, J. R. *Anal. Biochem.* **2004**, *324* (2), 170–182.
(117) Lakowicz, J. R. *Anal. Biochem.* **2005**, *337* (2), 171–194.
(118) Gryczynski, I.; Malicka, J.; Gryczynski, Z.; Lakowicz, J. R. *J. Phys. Chem. B* **2004**, *108* (33), 12568–12574.
(119) Wedge, S.; Wasey, J. a E.; Barnes, W. L.; Sage, I. *Appl. Phys. Lett.* **2004**, *85* (2004), 182–184.
(120) Andrew, P.; Barnes, W. L. *Science* **2004**, *306* (5698), 1002–1005.
(121) Cao, S.-H.; Cai, W.-P.; Liu, Q.; Li, Y.-Q. *Annu. Rev. Anal. Chem.* **2012**, *5* (1), 317–336.

(122) Zhang, Z. Z.; Wang, H. H.; Du, J. J.; Zhang, X. L.; Hao, Y. Y.; Chen, Q.; Sun, H. *IEEE Photonics Technol. Lett.* **2015**, *27* (8), 821–823.
(123) Cheng, Z.; Li, G.; Liu, M. *Sensors Actuators B Chem.* **2015**, *212*, 495–504.
(124) Chen, J.; Wang, K.; Wu, K.; Qian, L.; Long, H.; Wang, B.; Lu, P. *Opt. Commun.* **2015**, *349*, 180–184.
(125) Bhatnagar, K.; Pathak, a; Menke, D.; Cornish, P. V; Gangopadhyay, K.; Korampally, V.; Gangopadhyay, S. *Nanotechnology* **2012**, *23* (49), 495201.
(126) Miomandre, F.; Audibert, J. F.; Zhou, Q.; Audebert, P.; Martin, P.; Lacroix, J. C. *Electrochim. Acta* **2013**, *110*, 56–62.
(127) Tawa, K.; Hori, H.; Kintaka, K.; Kiyosue, K.; Tatsu, Y.; Nishii, J. *Opt. Express* **2008**, *16* (13), 9781–9790.
(128) Pokhriyal, A.; Lu, M.; Chaudhery, V.; Huang, C.-S.; Schulz, S.; Cunningham, B. T. *Opt. Express* **2010**, *18* (24), 24793–24808.
(129) Ekgasit, S.; Tangcharoenbumrungsuk, A.; Yu, F.; Baba, A.; Knoll, W. *Sens. Actuators, B* **2005**, *105* (2), 532–541.
(130) Toma, K.; Vala, M.; Adam, P.; Homola, J.; Knoll, W.; Dostálek, J. *Opt. Express* **2013**, *21* (8), 10121.
(131) White, I. M.; Fan, X. *Opt. Express* **2008**, *16* (2), 1020–1028.
(132) Homola, J.; Koudela, I.; Yee, S. S. *Sens. Actuators, B* **1999**, *54* (1–2), 16–24.
(133) Cui, X.; Tawa, K.; Hori, H.; Nishii, J. *Appl. Phys. Lett.* **2009**, *95* (13), 133117.
(134) Devaux, E.; Ebbesen, T. W.; Weeber, J. C.; Dereux, A. *Appl. Phys. Lett.* **2003**, *83* (24), 4936–4938.
(135) Barnes, W. L.; Dereux, A.; Ebbesen, T. W. *Nature* **2003**, *424* (6950), 824.
(136) Ekgasit, S.; Thammacharoen, C.; Knoll, W. *Anal. Chem.* **2004**, *76* (3), 561–568.
(137) Gupta, G.; Kondoh, J. *Sens. Actuators, B* **2007**, *122* (2), 381–388.
(138) Cai, D. B.; Lu, Y. H.; Lin, K. Q.; Wang, P.; Ming, H. *Opt. Express* **2008**, *16* (19), 14597–14602.
(139) Mu, W.; Buchholz, D. B.; Sukharev, M.; Jang, J. I.; Chang, R. P. H.; Ketterson, J. B. *Opt. Lett.* **2010**, *35* (4), 550.
(140) Singh, B. K.; Hillier, A. C. *Anal. Chem.* **2008**, *80* (10), 3803–3810.
(141) Chandezon, J.; Dupuis, M. T.; Cornet, G.; Maystre, D. *J. Opt. Soc. Am.* **1982**, *72* (7), 839–846.
(142) Dostálek, J.; Homola, J.; Miler, M. *Sensors Actuators B Chem.* **2005**, *107* (1), 154–161.
(143) Leveque, G.; Martin, O. J. F. *J. Appl. Phys.* **2006**, *100* (12), 6.
(144) Li, S.-Q.; Guo, P.; Buchholz, D. B.; Zhou, W.; Hua, Y.; Odom, T. W.; Ketterson, J. B.; Ocola, L. E.; Sakoda, K.; Chang, R. P. H. *ACS Photonics* **2014**, *1* (3), 163–172.
(145) Ekgasit, S.; Yu, F.; Knoll, W. *Sens. Actuators, B* **2005**, *104* (2), 294–301.
(146) Estevez, M. C.; Otte, M. A.; Sepulveda, B.; Lechuga, L. M. *Anal. Chim. Acta* **2014**, *806*, 55–73.
(147) Quail, J. C.; Rako, J. G.; Simon, H. J. *Opt. Lett.* **1983**, *8* (7), 377–379.
(148) Palik, E. D. *J. Opt. Soc. Am. A* **1984**, *1* (12), 1297.
(149) Yeh, W. **2013**.

CHAPTER 3

FLUORESCENCE ENHANCEMENT OF ABSORPTION AND EMISSION MODES OF RHODAMINE B IN POLY(METHYL METHACRYLATE) THROUGH SURFACE PLASMON COUPLED VIA SILVER GRATINGS

3.1 Abstract

This study explores the impact of grating coupled surface plasmon resonance enhancement of fluorescence. The fluorophore investigated was Rhodamine B dissolved in a thin layer of spin coated poly(methyl methacrylate). Investigation of surface plasmon coupled emission was performed by changing the exit polarization of light to the detector. Surface plasmon enhanced absorption was not performed in this study (an outline for future studies is provided). However, with the current results, there are serious implications of altering the fluorescence spectral emission shape – beyond purely enhancing the process – shown by intensifying fluorescence at some angles while possibly quenching fluorescence at other angles.

3.2 Introduction

Surface plasmon enhanced fluorescence, known as metal enhanced fluorescence (MEF) or radiative decay engineering by pioneers in the field, has several components through which a photoluminescence enhancement process occurs, as well as several complicating factors[59,109,110]. Key enhancement factors include decreased decay rate/increased quantum yield due to fluorophore-metal interactions, surface plasmon

enhanced absorption (SPEA) of light by the fluorophore, and surface plasmon coupled emission.

Surface plasmons (SPs) have been known to enhance the light absorbed by a molecule through increased electric field seen by the fluorophore and increased decay rates due to metal influence[109,111]. For example, tpically low emitting molecules like RNA and DNA have been shown to become visibly photoluminescent with the aid of surface plasmons, lending towards the application of rapid gene sequencing[109].

Additionally, emitted light from fluorophores can couple with plasmonic resonance modes through the process known as surface plasmon coupled emission (SPCE)[58,63,73,113,116,118,121,122]. Several qualities of interest exist for SPCE, included angle dependence of emission, meaning that photolumisence of fluorescent species will be enhanced at specific angles for fluorophores emitting at different wavelengths,[113,116,122] allowing for increased sensitivity for multiple fluorophores. An additional characteristic aspect includes polarization of the SPCE emitted light.[113,116,122]

Drawbacks of surface plasmon coupled emission include metal quenching of fluorophores within a certain distance (typically less than 20 nm) from the metal surface and loss of enhancement at further distances from the surface[109,111]. It is said that the emission from fluorophores outside of the evanescent field of the surface plasmon will be the same as a free space emitter[109]. For these reasons, the fluorophore must typically be, depending on penetration depth of the evanescent wave of the SP at a particular wavelength, between 20 and 500 nm of the metal surface.

In order to disperse fluorophores within the appropriate range from the metal surface, spin coating of fluorophore doped polymers are employed.[73,122] Examples of common

polymers include PMMA, PDMS, and PVA. Common fluorophores used include the rhodamine family (RhB, Rh-G6, etc)[53,123]. Alternatives to fluorophores include quantum dots such as Alq_3[84,113] or colloidal quantum dots.[73]

SPCE has been shown previously on grating based systems[84,113,121,122] and through reverse Kretschmann (RK) configurations[58,116,130]. These systems have established the merits of SPCE independent of SPEA. On the grating based systems, this was done by using a low wavelength excitation fluorophore such that surface coupling cannot occur at the excitation laser/absorption wavelength[113]. With the RK studies, SPCE was shown independent of SPEA by exciting a fluorophore on the ambient/air side of the metal film, and measuring the angle dependent emission on the prism side of the system[73,116].

The study shown here proposes to analyze both SPEA and SPCE by using a variable angle impingement and variable angle collection system with a polarizer and analyzer to polarize the excitation light source and detected light, respectively. Variable angle arms would allow for the determination of optimal angle for SPEA and SPCE and enhancement of fluorescence by SPEA and SPCE are confirmed and independently studied through the use of a polarizer and analyzer. However, due to limitations in time and laboratory equipment, a truncated study was performed and preliminary results are given.

3.3 Experimental Section

3.3.1 Materials

Silver wire (99.995% purity) and tungsten wire baskets for evaporation were acquired from Ted Pella (Redding, CA). The tin sputtering target (99.99% purity) was purchased from AJA International (North Scituate, MA). The UV curable polymer (NOA 61, Norland,

Cranbury, NJ) and polydimethylsiloxane silicone elastomer kit (SYLGARD 184, Dow Corning, Midland, MI) were used as received. Dow S1813 photoresist was purchased from Rohm and Haas Company (Philadelphia, PA) through Dow Chemicals (Midland, MI). Prefabricated low periodicity (556 nm and 417 nm) gratings were obtained from Lightsmyth (Eugene, OR). Toluene and glass microscope slides were obtained from Fisher (Waltham, MA). Poly(methyl methacrylate) (PMMA, 120,000 MW) and Rhodamine B (RhB, >95% HPLC) were purchased from Sigma-Aldrich (St. Louse, MO). Dionized water with electrical resistivity exceeding 18 MΩ*cm was used for cleaning and rinsing samples (NANOPure, Barnstead, Bubuque, IA).

3.3.2 Grating Fabrication.

Grating fabrication with laser interference lithography (LIL) followed a procedure as previously described[36] and will be briefly discussed here. A Lloyd's Mirror system was setup to imprint precise periodicity gratings through angle tuning. Rectangular gratings purchased from LightSmyth and LIL gratings were replicated onto clean glass slides with a UV curable polymer, as described in previous publications.[140,149] Gratings were subsequently coated via thermal evaporation with ~50 nm of silver, as monitored by a quartz crystal thickness monitor and confirmed through transmission studies.

3.3.3 PMMA/RhB Spin Preparation and Coating

A solution of 4% poly(methyl methacrylate) (PMMA) was made in toluene by dissolving under heat and stir-bar agitation overnight. A separate solution of 0.01 mg/mL solution of Rhodamine B (RhB) in ethanol had been previously prepared and diluted 1:10

with the PMMA solution (2 mL RhB solution added to 20 mL of PMMA solution). The solution was spin coated onto prepared gratings on glass slides at 4000 RPM for 45 seconds. Solvent was evaporated from the slides by placement on a hot plate for 10 minutes at 75ºC.

3.3.4 Optical Characterization

White light from a broadband halogen source (OSL1, Thorlabs Inc, New Jersey, USA) was used to analyze the spectral pass band of the Z532RDC dichroic beamsplitter (Chroma, Bellows Falls, Vermont, USA) and to obtain the absorption and emission curves for RhB. Fluorescence spectra were measured with a custom-built variable angle optical setup.[140,149] An Nd:YAG (neodymium-doped yttrium aluminium garnet; Nd:Y3Al5O12) laser (532 nm, 500 mW, Kaiser Optical, Ann Arbor, Michigan, USA) was used as the excitation source for the thin film fluorescence studies as it is outside the range of the band pass filter. A Glan-Thompson polarizer was used after the sample stage to analyze SPCE. The fluorescence light was collected with a 600 μm, bifurcated optical fiber that sent the light to two different spectrometers. An HR400CG spectrometer (Ocean Optics) was used to measure the spectral intensity at wavelengths between 350-1000 nm. Dispersion images were collected at angles ranging between -60° and +60° with respect to normal incidence using the motorized rotation stage in conjunction with a homebuilt control program (LabView), as described previously.[38]

3.4 Results and Discussion

3.4.1 Orientation to Results: Samples Analyzed and Spectral Results

Fluorescence of Rhodamine B (RhB) was spectrally interrogated through several platforms. First, a 10^{-5} mg/mL solution in ethanol was analyzed with white light. Then, a 4% (w/v) solutions of poly(methyl methacrylate) (PMMA) in toluene was prepared for spin coating thin layers of RhB rich polymer on our glass slide sensors. The weight percentage of the pre-spin coated solution was 0.01 mg/mL and the film thickness was roughly 120 nm. Fluorescence for these samples was excited with a 532 nm Nd:YAG laser and a 550-730 nm band pass filter. Two gratings were used for the spectra collected in this study: a homemade laser interference lithography (LIL) grating with a periodicity of 520 nm and a LightSmyth (LS) grating with a periodicity of 417 nm.

Results presented here contain in lab collection of absorbance and fluorescence of RhB in solution (Figure 3.1). Spectral bandpass of the dichroic mirror at two orthogonal post-polarization angles is presented in Figure 3.2. Spectra of the LIL and LS samples are separated into dispersion image analysis and fluorescence spectra collection. Dispersion images were obtained for both silver coated gratings with no film, PMMA spin-coated, and PMMA with RhB spin-coated. Finally, fluorescence spectra for the PMMA with RhB spin-coated samples are presented at select angles.

3.4.2 RhB in Ethanol Spectra and Band Pass Filter Analysis

Figure 3.1 shows absorption and emission curves for RhB in ethanol (A). White light shone into cuvettes with solutions were used to obtain both, with absorption collecting transmitted light using blank ethanol as a reference and emission collected using a 90^{o}

collection angle arrangement with white light impingement. For all laser studies, the bandpass filter discussed in the methods section was used.

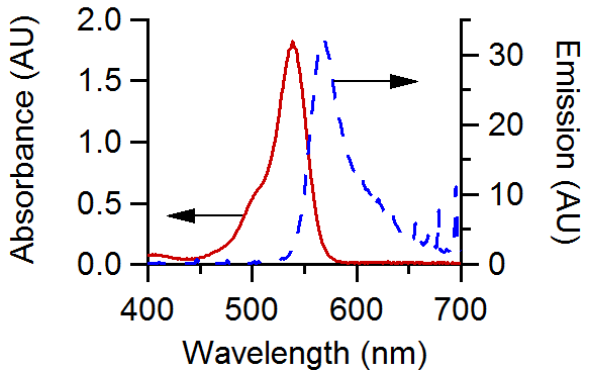

Figure 3.1 Absorption and emission curves for 10^{-5} mg/mL RhB in ethanol. A white light source was used for both meaurements. Absorbance was referenced with an ethanol solution and emission was collected via a 90^{o} collection angle.

The band pass range for white light through the dichroic mirror (550-730 nm) is shown in Figure 3.2. A polarizer on the detector side of the dichroic mirror was used to show negligible polarization dependence of the dichroic mirror. Excitation light from the Nd:YAG laser (532nm) is clearly outside the range of the band pass filter.

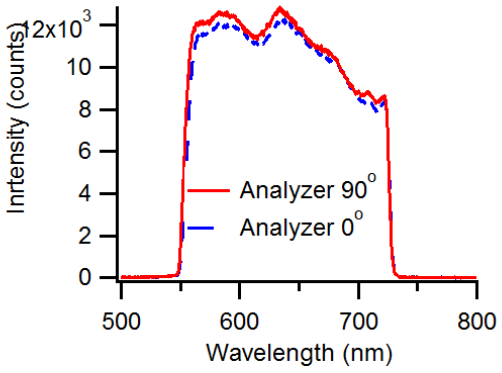

Figure 3.2 Band pass range for the dichroic mirror at orthogonal polarization angles.

3.4.3 Dispersion Images

The dispersion images for both LIL and LS gratings with silver (no PMMA), PMMA on silver, and PMMA with RhB on silver are shown in Figure 3.3. These give a basis for what to expect from the fluorescent studies.

The bare silver spectra show front and back side peak locations (Figure 3.3A/D). This is especially clear for the LIL fabricated grating (Figure 3.3A), where the bright bands crosses at around 550 nm are the front side SPR peaks and the dark bands at longer wavelengths and at larger angles are the back side peaks. With the deposition of PMMA or PMMA with RhB (Figure 3.4B/C/E/F) show that the front side peaks are nearly overlapping with the back side peaks, indicated by single bright bands where dark bands appeared on the bare silver dispersion images (Figure 3.4A/D).

It is unknown why the LS grating dispersion images are less symmetric and less clean than their LIL counterparts. It is thought that this may be due to differences in the grating profiles (LS is more rectangular, whereas LIL are sinusoidal) and subsequent difficulties in getting full coverage with evaporation and spin-coating techniques.

The dispersion images are meant to be a guide to indicate where we expect to see enhanced absorption and emission. However, as seen from analysis of fluorescence spectra (see Section 3.4.4), the angles of intense transmission on the dispersion images within the absorption and emission regime (500-600 nm) do not correlate with the angles of enhanced emission as seen by the fluorescence spectra (Figure 3.4 and Figure 3.5).

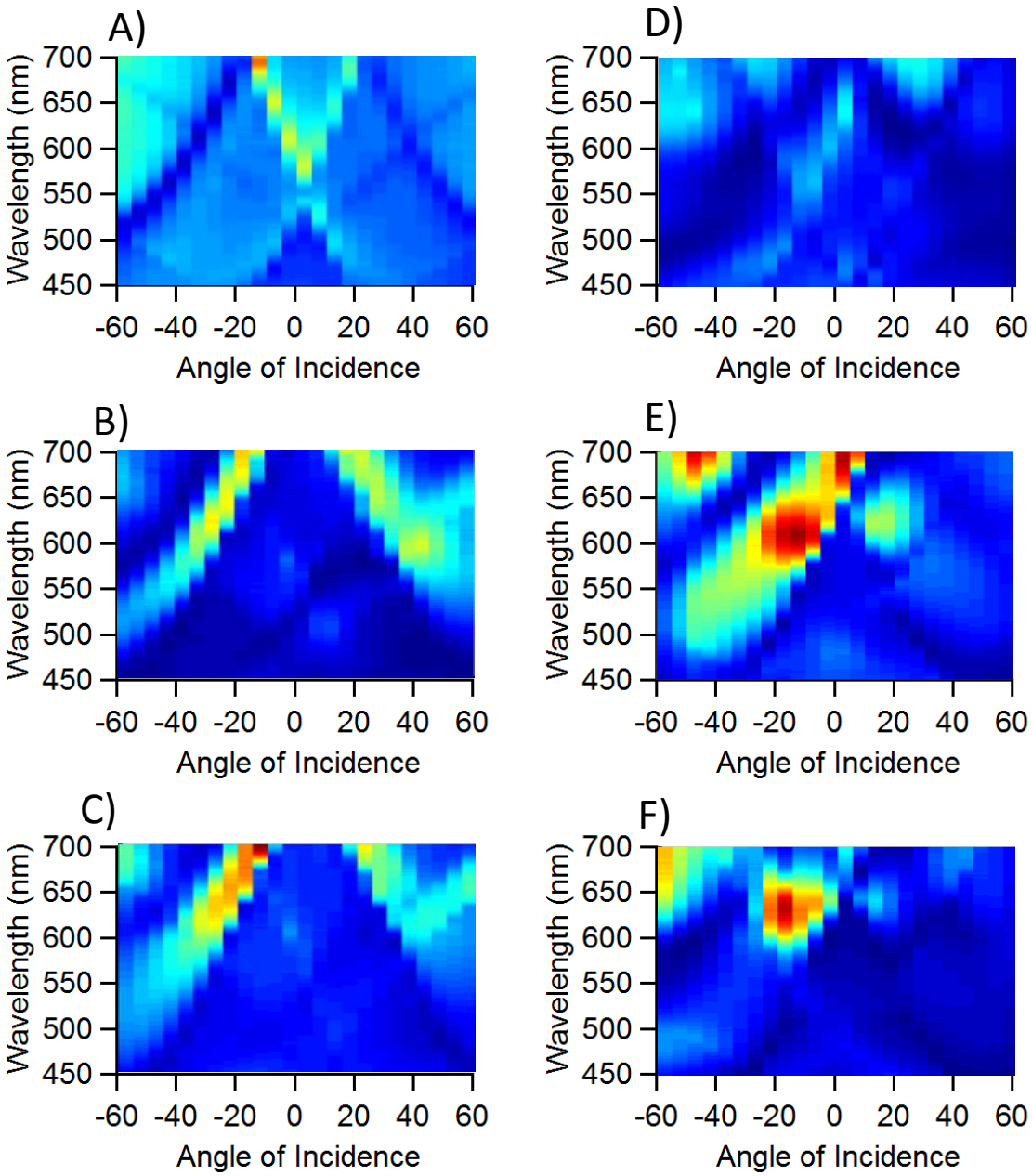

Figure 3.3 Dispersion images of LIL (520 nm – A/B/C) and LS (417 nm – D/E/F) gratings with silver (A/D), PMMA spin-coated (B/E), and PMMA with RhB spin coated (C/F).

3.4.4 Fluorescence Spectra

Figure 3.4 shows polarized emission spectra for the RhB in PMMA spin coated on the 520 nm LIL grating. At 0°, fluorescence is collected but there is minimal polarization dependance, meaning that SPCE is not a major mechanism for emission increase at this angle. However, at 15°, the spectra show polarization dependance enhanced emission, indicative of SPCE. While 15° shows SPCE clearly enhanced the emission maximum by 4.2-fold, all other angles produced minumal polarization dependent emission.

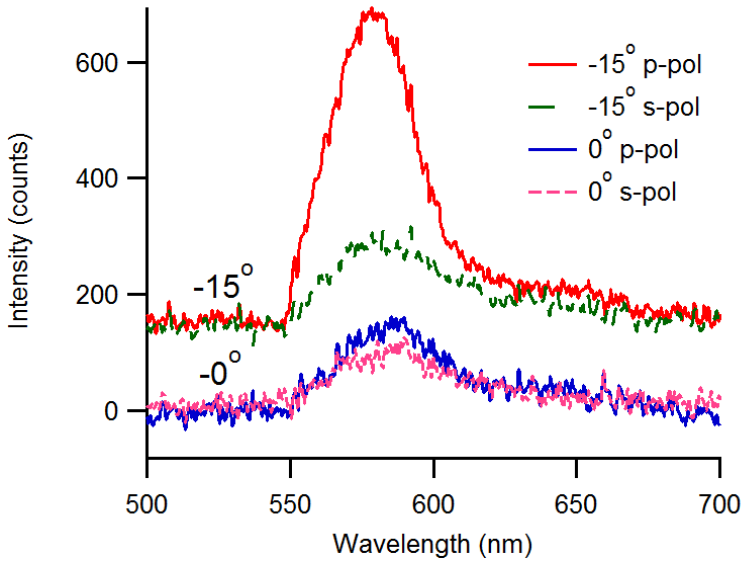

Figure 3.4 Polarized emission spectra for RhB in PMMA spin coated on the 520 nm LIL grating at 0° and 15°. SPCE observed strongly at 15°, with negligable SPCE at 0°.

Figure 3.5 shows polarized emission spectra for the RhB in PMMA spin coated on the 417 nm LS grating with RhB in PMMA spin coated. At 0°, SPCE is shown to enhance fluorescence 2.4-fold. The maximum angle of enhanced emission occurred at 7° with a SPCE 3.25-fold larger than non coupled emission (s-polarized). An interesting phenomena should be noted at 15°, however, showing decreased emission from the SPCE polarization plane.

This indicated that SPCE may not only enhance fluorophores at some matching, but also quench fluorescence at others. All other angles produced minumal polarization dependent emission.

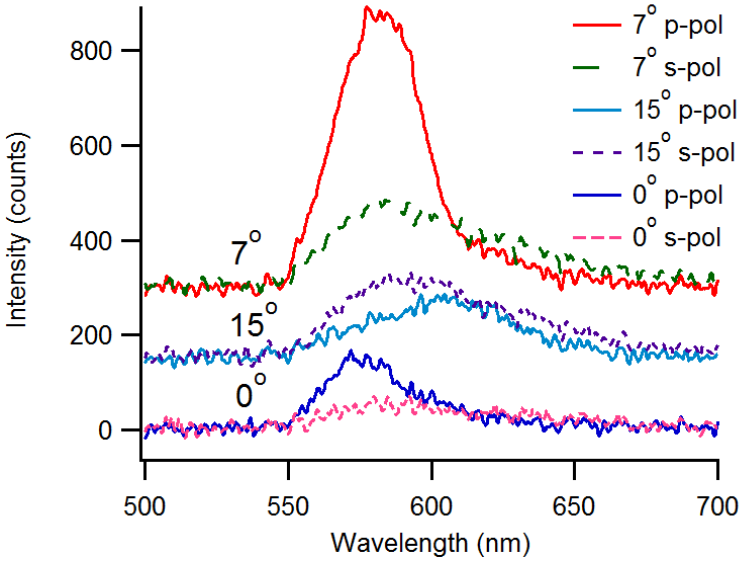

Figure 3.5 Polarized emission spectra for RhB in PMMA spin coated on the 417 nm LS grating at 0º, 7º and 15º. Strong SPCE observed at 7º, moderate SPCE observed at 0º, and fluorescence quenching observed at 7º.

3.5 Conclusion

Variable angle scans were performed through the use of a rotating stage in the path of a constant source and collection point (angle of impingement equals angle of collection, with reference to normal). For collection of dispersion images, this is the preferred orientation; however, varying the angle of both the excitation source and detector with variable polarization on either side is preferred for studies interrogating SPR enhanced fluorescence. However, a simple study was reported here.

This study was able to show polarization dependent emission spectra from a laser excited fluorophore. This indicates that the fluoresced light from RhB couples with a plasmon mode before being emitted to the detector. This coupled emission (SPCE) is

polarization dependent as this is characteristic for surface plasmon modes. Additional to showing a maximum enhancement of 4.2-fold, there are indications that grating based SPCE may be able to be used for quenching fluorophores at some angles of impingement, thus allowing for the turning on and off of a fluorophore by varying the angle of detection from the grating.

3.6 Proposed Study

The preferred experimental design would include additional information as outlined in the mock results below:

The study shown here analyzes both SEA (surface enhanced absorption) and SPCE (coupled emission) by using a variable angle impingement and collection system with a polarizer and analyzer to polarize the excitation light source and detected light, respectively. Variable angle arms allowed for the determination of optimal angle for SEA and SPCE. Enhancement of fluorescence due to SEA and SPCE are be confirmed, deconvoluted and independently studied through the use of the polarizer and analyzer

- Both polarizer and analyzer s-polarized with reference to grating should give free space emission profile (no MEF - metal enhanced fluorescence)
- Analyzer set to s-polarization and detector varied from p- to s-polarization will reveal effect of SEA
- Polarizer set to s-polarization and detector varied form p- to s-polarization will reveal effect of SPCE
- Varying both polarizer and analyzer at optimal angles will give cumulative effect of both SEA and SPCE

3.7 Acknowledgements

This work was supported by the National Science Foundation (Grant CHE 1213582).

3.8 References

(1) Wood, R. W. *Proc. Phys. Soc. London* **1902**, *18* (1), 269.
(2) Wood, R. W. *Philos. Mag. Ser. 6* **1912**, *23* (134), 310–317.
(3) Rayleigh, Lord. *Proc. R. Soc. London. Ser. A, Contain. Pap. a Math. Phys. Character* **1907**, *79* (532), 399–416.
(4) Hessel, A.; Oliner, A. A. *Appl. Opt.* **1965**, *4* (10), 1275.
(5) Ritchie, R. H. *Phys. Rev.* **1957**, *106* (5), 874–881.
(6) Powell, C. J.; Swan, J. B. *Phys. Rev.* **1960**, *118* (3), 640–643.
(7) Bohm, D.; Pines, D. *Phys. Rev.* **1951**, *82* (5), 625–634.
(8) Pines, D.; Bohm, D. *Phys. Rev.* **1952**, *85* (2), 338–353.
(9) Bohm, D.; Pines, D. *Phys. Rev.* **1953**, *92* (3), 609–625.
(10) Burstein, E. *J. Vac. Sci. Technol.* **1974**, *11* (6), 1004.
(11) Kretschmann, E.; Raether, H. *Zeitschrift Fuer Naturforschung, Tl. A* **1968**, *23* (November 1968), 2135.
(12) Kretschmann, E. *Zeitschrift für Phys.* **1971**, *241* (4), 313–324.
(13) Otto, A. *Zeitschrift für Phys.* **1968**, *216* (4), 398–410.
(14) Liedberg, B.; Nylander, C.; Lunström, I. *Sensors and Actuators* **1983**, *4*, 299–304.
(15) Pockrand, I.; Swalen, J. D.; Gordon, J. G.; Philpott, M. R. *Surf. Sci.* **1978**, *74* (1), 237–244.
(16) Peterlinz, K. A.; Georgiadis, R. *Opt. Commun.* **1996**, *130* (4-6), 260–266.
(17) Liedberg, B.; Lundström, I.; Stenberg, E. *Sensors Actuators B Chem.* **1993**, *11* (1-3), 63–72.
(18) Striebel, C.; Brecht, A.; Gauglitz, G. *Biosens. Bioelectron.* **1994**, *9* (2), 139–146.
(19) Cullen, D. C.; Brown, R. G. W.; Lowe, C. R.; Culle, D. C.; Brown, R. G. W.; Lowe, C. R. *Biosensors* **1987**, *3* (4), 211–225.
(20) Jory, M. J.; Bradberry, G. W.; Cann, P. S.; Sambles, J. R. *Meas. Sci. Technol.* **1995**, *6* (8), 1193.
(21) Lawrence, C. R.; Geddes, N. J.; Furlong, D. N.; Sambles, J. R. *Biosens. Bioelectron.* **1996**, *11* (4), 389–400.
(22) Moskovits, M. *Rev. Mod. Phys.* **1985**, *57* (3), 783–826.
(23) Willets, K. A.; Van Duyne, R. P. *Phys. Chem.* **2007**, *58*, 267–297.
(24) Haynes, C. L.; Van Duyne, R. P. *J. Phys. Chem. B* **2001**, *105* (24), 5599–5611.
(25) Homola, J.; Yee, S. S.; Gauglitz, G. *Sens. Actuators, B* **1999**, *54* (1–2), 3–15.
(26) Meneghello, A.; Antognoli, A.; Sonato, A.; Zacco, G.; Ruffato, G.; Cretaio, E.; Romanato, F. *Anal. Chem.* **2014**, *86* (23), 11773–11781.
(27) Yu, F.; Tian, S.; Yao, D.; Knoll, W. *Anal. Chem.* **2004**, *76* (13), 3530–3535.

(28) Silvestri, D.; Sonato, A.; Ruffato, G.; Meneghello, A.; Antognoli, A.; Cretaio, E.; Dettin, M.; Zamuner, A.; Casarin, E.; Zacco, G.; Romanato, F.; Morpurgo, M. *Anal. Methods* **2015**, *7* (10), 4173–4180.
(29) Singh, B. K.; Hillier, A. C. *Anal. Chem.* **2007**, *79* (14), 5124–5132.
(30) Wang, Y.; Brunsen, A.; Jonas, U.; Dostalek, J.; Knoll, W. *Anal. Chem.* **2009**, *81* (23), 9652.
(31) Zhu, H.; Snyder, M. *Curr. Opin. Chem. Biol.* **2003**, *7* (1), 55–63.
(32) Crespo-Biel, O.; Dordi, B.; Reinhoudt, D. N.; Huskens, J. *J. Am. Chem. Soc.* **2005**, *127* (20), 7594–7600.
(33) Jorgenson, R. C.; Yee, S. S. *Sens. Actuators, A* **1994**, *43* (1–3), 44–48.
(34) Mao, Y.; Bao, Y.; Wang, W.; Li, Z.; Li, F.; Niu, L. *Talanta* **2011**, *85* (4), 2106–2112.
(35) Pei, R. J.; Cui, X. Q.; Yang, X. R.; Wang, E. K. *Biomacromolecules* **2001**, *2* (2), 463–468.
(36) Petefish, J. W.; Hillier, A. C. *Anal. Chem.* **2014**, *86* (5), 2610–2617.
(37) Singh, B. K.; Hillier, A. C. *Anal. Chem.* **2006**, *78* (20), 7335–7340.
(38) Yeh, W.-H.; Hillier, A. C. *Anal. Chem.* **2013**, *85* (8), 4080–4086.
(39) Yeh, W.-H.; Petefish, J. W.; Hillier, A. C. *Anal. Chem.* **2011**, *83* (15), 6047–6053.
(40) Yeh, W.-H.; Petefish, J. W.; Hillier, A. C. *Anal. Chem.* **2012**, *84* (2), 1139–1145.
(41) Homola, J. *Anal. Bioanal. Chem.* **2003**, *377* (3), 528–539.
(42) Couture, M.; Zhao, S. S.; Masson, J.-F. *Phys. Chem. Chem. Phys.* **2013**, *15* (27), 11190–11216.
(43) Homola, J. J. *Chem. Rev.* **2008**, *108* (2), 462–493.
(44) Cooper, M. A. *Nature Reviews Drug Discovery*. 2002, pp 515–528.
(45) Myszka, D. G. *J. Mol. Recognit.* **1999**, *12* (5), 279–284.
(46) Huang, Y.-F.; Zhang, M.; Zhao, L.-B.; Feng, J.-M.; Wu, D.-Y.; Ren, B.; Tian, Z.-Q. *Angew. Chemie Int. Ed.* **2014**, *53* (9), 2353–2357.
(47) Lal, S.; Grady, N. K.; Kundu, J.; Levin, C. S.; Lassiter, J. B.; Halas, N. J. *Chem. Soc. Rev.* **2008**, *37* (5), 898–911.
(48) Nie, S.; Emory, S. R. *Science (80-.).* **1997**, *275* (5303), 1102–1106.
(49) Campion, A.; Kambhampati, P.; Campion, A.; Kambhampati, P. *Chem. Soc. Rev.* **1998**, *27* (4), 241–250.
(50) Zhou, F.; Liu, Y.; Cai, W. *Opt. Lett.* **2014**, *39* (5), 1302–1305.
(51) Miyake, H.; Ye, S.; Osawa, M. *Electrochem. Commun.* **2002**, *4* (12), 973–977.
(52) Le, F.; Brandl, D. W.; Urzhumov, Y. A.; Wang, H.; Kundu, J.; Halas, N. J.; Aizpurua, J.; Nordlander, P. *ACS Nano* **2008**, *2* (4), 707–718.
(53) Smolyaninov, I. I.; Hung, Y. J.; Davis, C. C. *Conf. Quantum Electron. Laser Sci. - Tech. Dig. Ser.* **2007**, *14* (22), 10825–10830.
(54) Huang, C.-J.; Dostalek, J.; Sessitsch, A.; Knoll, W. *Anal. Chem.* **2011**, *83* (3), 674–677.
(55) Chun Jen, H.; Jakub, D.; Wolfgang, K. *J. Vac. Sci. Technol., B Microelectron. Nanom. Struct.* **2010**, *28*, 66.
(56) Ekgasit, S.; Thammacharoen, C.; Yu, F.; Knoll, W. *Anal. Chem.* **2004**, *76* (8), 2210–2219.
(57) Kasry, A.; Knoll, W. *Appl. Phys. Lett.* **2006**, *89* (10), 101103–101106.
(58) Lakowicz, J. R. *Anal. Biochem.* **2004**, *324* (2), 153–169.

(59) Bauch, M.; Toma, K.; Toma, M.; Zhang, Q.; Dostalek, J. *Plasmonics* **2014**, *9* (4), 781–799.
(60) Lakowicz, J. R.; Ray, K.; Chowdhury, M.; Szmacinski, H.; Fu, Y.; Zhang, J.; Nowaczyk, K. *Analyst* **2008**, *133* (10), 1308.
(61) Ekgasit, S.; Yu, F.; Knoll, W.; Biosensor, S. *Langmuir* **2005**, *21* (9), 4077–4082.
(62) Hecht, B.; Sick, B.; Wild, U. P.; Deckert, V.; Zenobi, R.; Martin, O. J. F.; Pohl, D. W. *J. Chem. Phys.* **2000**, *112* (18), 7761–7774.
(63) Qiu, D.; Zhang, D.; Chen, Y.; Zhu, L.; Han, L.; Wang, P.; Ming, H.; Badugu, R.; Lakowicz, J. R. *Opt. Lett.* **2014**, *39* (15), 4341–4344.
(64) Beck, F. J.; Polman, A.; Catchpole, K. R. *J. Appl. Phys.* **2009**, *105* (11), 114310–114317.
(65) Kamat, P. V. *J. Phys. Chem. C* **2007**, *111* (7), 2834–2860.
(66) Linic, S.; Christopher, P.; Ingram, D. B. *Nat Mater* **2011**, *10* (12), 911–921.
(67) Pillai, S.; Catchpole, K. R.; Trupke, T.; Green, M. A. *J. Appl. Phys.* **2007**, *101* (9), 93105–93108.
(68) Yoon, W.-J.; Jung, K.-Y.; Liu, J.; Duraisamy, T.; Revur, R.; Teixeira, F. L.; Sengupta, S.; Berger, P. R. *Sol. Energy Mater. Sol. Cells* **2010**, *94* (2), 128–132.
(69) West, P. R.; Ishii, S.; Naik, G. V.; Emani, N. K.; Shalaev, V. M.; Boltasseva, A. *Laser Photonics Rev.* **2010**, *4* (6), 795–808.
(70) Kretschmann, E. *Opt. Commun.* **1972**, *5* (5), 331–336.
(71) Ritchie, R. H. *Phys. status solidi* **1970**, *39* (1), 297–308.
(72) Nagpal, P.; Lindquist, N. C.; Oh, S.-H.; Norris, D. J. *Science (80-.).* **2009**, *325* (5940), 594–597.
(73) Gryczynski, I.; Malicka, J.; Jiang, W.; Fischer, H.; Chan, W. C. W.; Gryczynski, Z.; Grudzinski, W.; Lakowicz, J. R. *J. Phys. Chem. B* **2005**, *109* (1), 1088–1093.
(74) Abbas, A.; Linman, M.; Cheng, Q. *Biosens. Bioelectron.* **2011**, *26* (5), 1815–1824.
(75) Kaplan, B.; Guner, H.; Senlik, O.; Gurel, K.; Bayindir, M.; Dana, A. *Plasmonics* **2009**, *4* (3), 237–243.
(76) Giannattasio, A.; Barnes, W. *Opt. Express* **2005**, *13* (2), 428–434.
(77) Magnusson, R.; Svavarsson, H. G.; Yoon, J.; Shokooh-Saremi, M.; Song, S. H. *Appl. Phys. Lett.* **2013**, *100* (9), 091106.
(78) Chang, S.-H.; Gray, S.; Schatz, G. *Opt. Express* **2005**, *13* (8), 3150–3165.
(79) Halpern, A. R.; Corn, R. M. *ACS Nano* **2013**, *7* (2), 1755–1762.
(80) Lindquist, N. C.; Nagpal, P.; Lesuffleur, A.; Norris, D. J.; Oh, S.-H. *Nano Lett.* **2010**, *10* (4), 1369–1373.
(81) Chung, A. J.; Huh, Y. S.; Erickson, D. *Nanoscale* **2011**, *3* (7), 2903–2908.
(82) Wang, S.; Pile, D. F. P.; Sun, C.; Zhang, X. *Nano Lett.* **2007**, *7* (4), 1076–1080.
(83) Franzen, S. *J. Phys. Chem. C* **2008**, *112* (15), 6027–6032.
(84) Chiu, N.-F.; Lin, C.; Lee, J.-H.; Kuan, C.; Wu, K.; Lee, C.; Yu, C.; Nien, S.-Y.; Lee, J.-H.; Kuan, C.; Wu, K.; Lee, C.; Lin, C.; Nan-Fu, C.; Chii-Wann, L.; Jiun-Haw, L.; Chieh-Hsiung, K.; Kuang-Chong, W.; Chih-Kung, L. *Appl. Phys. Lett.* **2007**, *91* (8), 83114.
(85) Petefish, J. **2014**.
(86) Chegel, V.; Whitcombe, M. J.; Turner, N. W.; Piletsky, S. A. *Biosens. Bioelectron.* **2009**, *24* (5), 1270–1275.
(87) Moharam, M. G.; Gaylord, T. K. *J. Opt. Soc. Am. A* **1986**, *3* (11), 1780–1787.

(88) Moharam, M. G.; Grann, E.; Pommet, D.; Gaylord, T. K. *J. Opt. Soc. Am. A* **1995**, *12* (5), 1068–1076.
(89) Moharam, M. G.; Pommet, D.; Grann, E.; Gaylord, T. K. *J. Opt. Soc. Am. A* **1995**, *12* (5), 1077–1086.
(90) Knoll, W. *Annu. Rev. Phys. Chem.* **1998**, *49* (1), 569–638.
(91) MAIER, S. A. *Plasmonics: Fundamentals and Applications*; Springer: 233 Spring Street, New York, NY 10013, USA, 2007; Vol. 1.
(92) Boersch, H.; Geiger, J.; Imbusch, A.; Niedrig, N. *Phys. Lett.* **1966**, *22* (2), 146–147.
(93) Sarid, D. *Phys. Rev. Lett.* **1981**, *47* (26), 1927–1930.
(94) Stegeman, G. I.; Burke, J. J.; Hall, D. G. *Opt. Lett.* **1983**, *8* (7), 383.
(95) Burke, J. J.; Stegeman, G. I.; Tamir, T. *Phys. Rev. B* **1986**, *33* (8), 5186–5201.
(96) Wang, Y.; Knoll, W.; Dostalek, J. *Anal. Chem.* **2012**, *84* (19), 8345–8350.
(97) Dostálek, J.; Roskamp, R. F.; Knoll, W. *Sensors Actuators B Chem.* **2009**, *139* (1), 9–12.
(98) Nenninger, G. G.; Tobiška, P.; Homola, J.; Yee, S. S. *Sens. Actuators, B* **2001**, *74* (1–3), 145–151.
(99) Dostálek, J.; Kasry, A.; Knoll, W. *Plasmonics* **2007**, *2* (3), 97–106.
(100) Joo, Y. H.; Song, S. H.; Magnusson, R. *Opt. Express* **2009**, *17* (13), 10606.
(101) Huang, C. J.; Dostalek, J.; Knoll, W. *Biosens. Bioelectron.* **2010**, *26* (4), 1425–1431.
(102) Ishikawa-Ankerhold, H. C.; Ankerhold, R.; Drummen, G. *Molecules*. 2012, pp 4047–4132.
(103) Noomnarm, U.; Clegg, R. *Off. J. Int. Soc. Photosynth. Res.* **2009**, *101* (2), 181–194.
(104) *Curr. Biol.* **1994**, *4* (5), 443.
(105) Yang, T.-T.; Kain, S. R.; Kitts, P.; Kondepudi, A.; Yang, M. M.; Youvan, D. C. *Gene* **1996**, *173* (1), 19–23.
(106) Chen, W.; Long, K. D.; Yu, H.; Tan, Y.; Choi, J. S.; Harley, B. a; Cunningham, B. T. *Analyst* **2014**, *139* (22), 5954–5963.
(107) Basché, T. *J. Lumin.* **1998**, *76-77*, 263–269.
(108) Patterson, G. H. *Semin. Cell Dev. Biol.* **2009**, *20* (8), 886–893.
(109) Geddes, C. D.; Lakowicz, J. R. *J. Fluoresc.* **2002**, *12* (2), 121–129.
(110) Szmacinski, H.; Lakowicz, J. R. *Anal. Chem.* **2008**, *80* (16), 6260–6266.
(111) Liebermann, T.; Knoll, W. *Colloids Surf., A* **2000**, *171* (1–3), 115–130.
(112) Kim, K.; Kim, D. J.; Kim, D. *Quantum Dots, Part. Nanoclusters Vi* **2009**, *7224*, SPIE.
(113) Hao, Y.; Wang, H.; Zhang, Z.; Zhang, X. L.; Chen, Q.; Sun, H. *J. Phys. Chem. C* **2013**, *117* (50), 26734–26739.
(114) Neumann, T.; Johansson, M.-L.; Kambhampati, D.; Knoll, W. *Adv. Funct. Mater.* **2002**, *12* (9), 575–586.
(115) Lakowicz, J. R.; Shen, Y.; D'Auria, S.; Malicka, J.; Fang, J.; Gryczynski, Z.; Gryczynski, I. *Anal. Biochem.* **2002**, *301* (2), 261–277.
(116) Gryczynski, I.; Malicka, J.; Gryczynski, Z.; Lakowicz, J. R. *Anal. Biochem.* **2004**, *324* (2), 170–182.
(117) Lakowicz, J. R. *Anal. Biochem.* **2005**, *337* (2), 171–194.
(118) Gryczynski, I.; Malicka, J.; Gryczynski, Z.; Lakowicz, J. R. *J. Phys. Chem. B* **2004**, *108* (33), 12568–12574.
(119) Wedge, S.; Wasey, J. a E.; Barnes, W. L.; Sage, I. *Appl. Phys. Lett.* **2004**, *85* (2004), 182–184.

(120) Andrew, P.; Barnes, W. L. *Science* **2004**, *306* (5698), 1002–1005.
(121) Cao, S.-H.; Cai, W.-P.; Liu, Q.; Li, Y.-Q. *Annu. Rev. Anal. Chem.* **2012**, *5* (1), 317–336.
(122) Zhang, Z. Z.; Wang, H. H.; Du, J. J.; Zhang, X. L.; Hao, Y. Y.; Chen, Q.; Sun, H. *IEEE Photonics Technol. Lett.* **2015**, *27* (8), 821–823.
(123) Cheng, Z.; Li, G.; Liu, M. *Sensors Actuators B Chem.* **2015**, *212*, 495–504.
(124) Chen, J.; Wang, K.; Wu, K.; Qian, L.; Long, H.; Wang, B.; Lu, P. *Opt. Commun.* **2015**, *349*, 180–184.
(125) Bhatnagar, K.; Pathak, a; Menke, D.; Cornish, P. V; Gangopadhyay, K.; Korampally, V.; Gangopadhyay, S. *Nanotechnology* **2012**, *23* (49), 495201.
(126) Miomandre, F.; Audibert, J. F.; Zhou, Q.; Audebert, P.; Martin, P.; Lacroix, J. C. *Electrochim. Acta* **2013**, *110*, 56–62.
(127) Tawa, K.; Hori, H.; Kintaka, K.; Kiyosue, K.; Tatsu, Y.; Nishii, J. *Opt. Express* **2008**, *16* (13), 9781–9790.
(128) Pokhriyal, A.; Lu, M.; Chaudhery, V.; Huang, C.-S.; Schulz, S.; Cunningham, B. T. *Opt. Express* **2010**, *18* (24), 24793–24808.
(129) Ekgasit, S.; Tangcharoenbumrungsuk, A.; Yu, F.; Baba, A.; Knoll, W. *Sens. Actuators, B* **2005**, *105* (2), 532–541.
(130) Toma, K.; Vala, M.; Adam, P.; Homola, J.; Knoll, W.; Dostálek, J. *Opt. Express* **2013**, *21* (8), 10121.
(131) White, I. M.; Fan, X. *Opt. Express* **2008**, *16* (2), 1020–1028.
(132) Homola, J.; Koudela, I.; Yee, S. S. *Sens. Actuators, B* **1999**, *54* (1–2), 16–24.
(133) Cui, X.; Tawa, K.; Hori, H.; Nishii, J. *Appl. Phys. Lett.* **2009**, *95* (13), 133117.
(134) Devaux, E.; Ebbesen, T. W.; Weeber, J. C.; Dereux, A. *Appl. Phys. Lett.* **2003**, *83* (24), 4936–4938.
(135) Barnes, W. L.; Dereux, A.; Ebbesen, T. W. *Nature* **2003**, *424* (6950), 824.
(136) Ekgasit, S.; Thammacharoen, C.; Knoll, W. *Anal. Chem.* **2004**, *76* (3), 561–568.
(137) Gupta, G.; Kondoh, J. *Sens. Actuators, B* **2007**, *122* (2), 381–388.
(138) Cai, D. B.; Lu, Y. H.; Lin, K. Q.; Wang, P.; Ming, H. *Opt. Express* **2008**, *16* (19), 14597–14602.
(139) Mu, W.; Buchholz, D. B.; Sukharev, M.; Jang, J. I.; Chang, R. P. H.; Ketterson, J. B. *Opt. Lett.* **2010**, *35* (4), 550.
(140) Singh, B. K.; Hillier, A. C. *Anal. Chem.* **2008**, *80* (10), 3803–3810.
(141) Chandezon, J.; Dupuis, M. T.; Cornet, G.; Maystre, D. *J. Opt. Soc. Am.* **1982**, *72* (7), 839–846.
(142) Dostálek, J.; Homola, J.; Miler, M. *Sensors Actuators B Chem.* **2005**, *107* (1), 154–161.
(143) Leveque, G.; Martin, O. J. F. *J. Appl. Phys.* **2006**, *100* (12), 6.
(144) Li, S.-Q.; Guo, P.; Buchholz, D. B.; Zhou, W.; Hua, Y.; Odom, T. W.; Ketterson, J. B.; Ocola, L. E.; Sakoda, K.; Chang, R. P. H. *ACS Photonics* **2014**, *1* (3), 163–172.
(145) Ekgasit, S.; Yu, F.; Knoll, W. *Sens. Actuators, B* **2005**, *104* (2), 294–301.
(146) Estevez, M. C.; Otte, M. A.; Sepulveda, B.; Lechuga, L. M. *Anal. Chim. Acta* **2014**, *806*, 55–73.
(147) Quail, J. C.; Rako, J. G.; Simon, H. J. *Opt. Lett.* **1983**, *8* (7), 377–379.
(148) Palik, E. D. *J. Opt. Soc. Am. A* **1984**, *1* (12), 1297.
(149) Yeh, W. **2013**.